

# The Occurrence-weighted Median Planets Discovered by Transit Surveys Orbiting Solar-type Stars and Their Implications for Planet Formation and Evolution

KEVIN C. SCHLAUFMAN<sup>1</sup> AND NOAH D. HALPERN<sup>1</sup>

<sup>1</sup>*Department of Physics and Astronomy  
Johns Hopkins University  
3400 N Charles St  
Baltimore, MD 21218, USA*

(Received August 4, 2020; Revised June 14, 2021; Accepted June 15, 2021)

Accepted for publication in the *Astrophysical Journal*

## ABSTRACT

Since planet occurrence and primordial atmospheric retention probability increase with period, the occurrence-weighted median planets discovered by transit surveys may bear little resemblance to the low-occurrence, short-period planets sculpted by atmospheric escape ordinarily used to calibrate mass–radius relations and planet formation models. An occurrence-weighted mass–radius relation for the low-mass planets discovered so far by transit surveys orbiting solar-type stars requires both occurrence-weighted median Earth-mass and Neptune-mass planets to have a few percent of their masses in hydrogen/helium (H/He) atmospheres. Unlike the Earth that finished forming long after the protosolar nebula was dissipated, these occurrence-weighted median Earth-mass planets must have formed early in their systems’ histories. The existence of significant H/He atmospheres around Earth-mass planets confirms an important prediction of the core-accretion model of planet formation. It also implies core masses  $M_c$  in the range  $2 M_\oplus \lesssim M_c \lesssim 8 M_\oplus$  that can retain their primordial atmospheres. If atmospheric escape is driven by photoevaporation due to extreme ultraviolet (EUV) flux, then our observation requires a reduction in the fraction of incident EUV flux converted into work usually assumed in photoevaporation models. If atmospheric escape is core driven, then the occurrence-weighted median Earth-mass planets must have large Bond albedos. In contrast to Uranus and Neptune that have at least 10% of their masses in H/He atmospheres, these occurrence-weighted median Neptune-mass planets are H/He poor. The implication is that they experienced collisions or formed in much shorter-lived and/or hotter parts of their parent protoplanetary disks than Uranus and Neptune’s formation location in the protosolar nebula.

*Keywords:* Exoplanet atmospheres(487) — Exoplanet evolution(491) — Exoplanet formation(492) — Exoplanets(498) — Mini Neptunes(1063) — Super Earths(1655)

## 1. INTRODUCTION

The observable properties of the host stars of transiting planets can be used to infer both the masses and radii of their transiting planets. The radius of a planet with a given mass can then be used as a diagnostic of its composition and consequently its formation and evo-

lution. Studies of planet occurrence around both solar-type and late-type dwarfs in the Kepler field as a function of orbital period  $P$  and planet radius  $R_p$  have revealed that long-period, small-radius planets are much more common outcomes of planet formation than short-period, large-radius planets (e.g., [Fressin et al. 2013](#); [Dressing & Charbonneau 2013, 2015](#); [Hsu et al. 2019, 2020](#)). Though these long-period, small-radius planets are more representative of the Galaxy’s planet population, the number of planets discovered in a photon-noise limited transit survey  $N_p$  is proportional to semimajor

Corresponding author: Kevin C. Schlaufman  
[kschlaufman@jhu.edu](mailto:kschlaufman@jhu.edu)

axis  $a$  and  $R_p$  as  $a^{-5/2} R_p^6$  (Pepper et al. 2003). In addition to being relatively uncommon among transit discoveries, at constant mass it is more difficult to infer masses using the Doppler technique or transit-timing variations (TTVs) for these high-occurrence, long-period, small-radius planets than for low-occurrence, short-period, large-radius planets. The amplitude of the Doppler reflex velocity  $K$  for a star hosting a planet with mass  $M_p$  is proportional to  $M_p P^{-1/3}$ , dropping below  $K = 3 \text{ m s}^{-1}$  for a planet with  $M_p = 10 M_\oplus$  at  $P = 10$  days. The signal-to-noise ratio S/N in a TTV measurement is proportional to  $M_p R_p^{3/2} P^{5/6}$  in general and  $M_p R_p^{3/2} P^{1/3}$  in the duration-limited case appropriate for Kepler, K2, and the Transiting Exoplanet Survey Satellite (TESS) continuous-viewing zones (Steffen 2016; Mills & Mazeh 2017). The net result of these observational selection effects is that high-occurrence, long-period, small-radius planets are underrepresented in the existing sample of small planets with inferred masses.

The underrepresentation of high-occurrence, long-period, small-radius planets in the existing sample of mass inferences is an obstacle to the use of inferred exoplanet masses and radii to calibrate models of planet formation and evolution. Mass and radius inferences are most constraining for low-mass planets, as masses and radii do not uniquely define the compositions of more massive planets (e.g., Adams et al. 2008). While mass and radius measurements for short-period planets are powerful probes of planet evolution, the susceptibility of primordial hydrogen/helium (H/He) atmospheres to atmospheric escape make it more difficult to discern the properties of low-mass, short-period planets immediately after the end of the planet formation process (e.g., Youdin 2011; Lopez et al. 2012; Lopez & Fortney 2013, 2014; Owen & Wu 2013, 2016, 2017; Wu & Lithwick 2013; Ginzburg et al. 2016, 2018).

Despite these difficulties, the relationship between planet masses and radii has been quantified with increasing statistical sophistication for planets orbiting both solar-type and late-type dwarfs (e.g., Lissauer et al. 2011a; Wu & Lithwick 2013; Weiss & Marcy 2014; Hadden & Lithwick 2014; Wolfgang et al. 2016; Mills & Mazeh 2017; Chen & Kipping 2017; Ning et al. 2018; Kanodia et al. 2019; Ulmer-Moll et al. 2019; Neil & Rogers 2020; Otegi et al. 2020; Teske et al. 2020a). While these studies acknowledged the underrepresentation of high-occurrence, long-period, small-radius planets in their analysis samples, their goals did not require correcting for it. Many of these studies conflated planets orbiting solar-type and late-type dwarfs (Wu & Lithwick 2013; Weiss & Marcy 2014; Hadden & Lithwick 2014; Wolfgang et al. 2016; Chen & Kipping 2017; Ning

et al. 2018; Ulmer-Moll et al. 2019; Otegi et al. 2020; Teske et al. 2020a) even though it has become clear that the outcome of planet formation depends on host star mass (e.g., Laughlin et al. 2004; Ida & Lin 2005). A few of these studies chose to focus either on Doppler (Neil & Rogers 2020) or TTV mass inferences (Hadden & Lithwick 2014). Several limited the range of planetary radii considered, thereby ignoring low-mass, large-radius planets like those in the Kepler-51 system (Weiss & Marcy 2014; Hadden & Lithwick 2014; Wolfgang et al. 2016; Ning et al. 2018). Some studied only planets with precise mass and radius inferences, biasing their results against low-density planets for which precise mass measurements are more challenging (Otegi et al. 2020).

In this paper, we assemble a sample of masses and radii for transiting planets orbiting single solar-type stars with Doppler-, TTV-, or joint Doppler/TTV-inferred masses consistent with  $M_p \leq 20 M_\oplus$  without regard to planetary radii. We leverage the known occurrence of planets as a function of period and radius to derive occurrence-weighted mass–radius, radius–mass, mass–density, and radius–density relations. While weighting the analysis sample by occurrence does not completely eliminate the biases of the transit, Doppler, or TTV techniques, it does mitigate those effects using currently available data. The resulting relations provide a better view of the usual outcome of planet formation in the Galaxy than the existing mass–radius relations in the literature and should provide more accurate constraints for theoretical models of planet formation. We describe the construction of our sample of masses and radii in Section 2. We detail in Section 3 our analysis procedure and a theoretical model that allows us to interpret our results in the planet formation context. We review our results and their implications for planet formation and evolution in Section 4. We conclude by summarizing our findings in Section 5.

## 2. DATA

We queried the NASA Exoplanet Archive (Akeson et al. 2013) on 14 June 2021 for all transiting exoplanets with Doppler data or TTVs. We first removed all circumbinary planets. We then queried SIMBAD to find the Gaia Data Release 2 (DR2) source ID and SIMBAD default name of every host star. We next used those Gaia DR2 source IDs to query the ESA Gaia Archive for each host star’s photometric and astrometric properties (Gaia Collaboration et al. 2016, 2018; Arenou et al. 2018; Evans et al. 2018; Hambly et al. 2018; Luri et al. 2018; Riello et al. 2018; Marrese et al. 2019). We dereddened each star’s Gaia  $G_{BP} - G_{RP}$  color using the three-dimensional reddening map from Lalle-

ment et al. (2018) assuming Gaia DR2 extinction coefficients from Casagrande & Vandenberg (2018) and prior-informed stellar distances from Bailer-Jones et al. (2018). We retained only planets orbiting solar-type stars with  $0.58 < (G_{\text{BP}} - G_{\text{RP}})_0 < 1.41$ , roughly corresponding to dwarf stars with effective temperature  $T_{\text{eff}}$  in the range  $4500 \text{ K} \lesssim T_{\text{eff}} \lesssim 6500 \text{ K}$  or equivalently dwarf stars with spectral types between F5V and K5V (e.g., Pecaut & Mamajek 2013)<sup>1</sup>. We used dereddened Gaia  $(G_{\text{BP}} - G_{\text{RP}})_0$  color to focus on solar-type stars instead of inferred stellar masses  $M_*$  or  $T_{\text{eff}}$  because for every exoplanet host star in our initial sample high-precision Gaia DR2 photometry is available and  $(G_{\text{BP}} - G_{\text{RP}})_0$  can be homogeneously inferred.

We analyze masses inferred using both the Doppler and TTV techniques, as there is no reason to believe that the two methods produce systematically different mass inferences (e.g., Mills & Mazeh 2017). To ensure the homogeneity of the mass inferences in our analysis sample to the greatest extent possible, we prefer mass estimates based on Kepler TTVs from the large, homogeneous Kepler TTV analysis of Hadden & Lithwick (2017) when they have not been superseded by subsequent analyses. If Hadden & Lithwick (2017) found that it was not possible to robustly infer the mass of a planet with a previously published TTV-based mass estimate, then we excluded that planet from our analysis sample. We also excluded planets with published TTV-based mass estimates from Xie (2014) and Hadden & Lithwick (2014) that were not reproduced in Hadden & Lithwick (2017), as those mass inferences were based on analytic relations from Lithwick et al. (2012) and therefore were forced to make assumptions about the unknown free eccentricity distributions in their samples. Since the TTV-based mass estimates of Hadden & Lithwick (2017) and Saad-Oliveira et al. (2017) were calculated without regard to planet radius, we updated the radii and radius uncertainties for the planets analyzed in those papers based on Kepler DR25 transit depths (Thompson et al. 2018) and host star radii inferences from Brewer & Fischer (2018), Johnson et al. (2017), or Berger et al. (2020) in that order. Because our focus is on planets with  $M_p \lesssim 20 M_{\oplus}$ , we excluded all planets with masses that are not consistent with  $M_p \leq 20 M_{\oplus}$  at the  $3\text{-}\sigma$  level or with only mass upper limits. Our final analysis sample includes 201 planets orbiting single solar-type stars: 133 planets with Doppler mass inferences, 58 planets with TTV mass inferences, and 10 planets with masses from joint Doppler/TTV analyses.

We calculated the occurrence of each planet in our analysis sample by linearly interpolating Table 2 of Hsu et al. (2019) that gives planet occurrence as a function of period and radius when considering both detection and vetting efficiency. We plot our analysis sample in Figure 1 and list each planet in the analysis sample sorted in decreasing order of planet occurrence in Table 1. For multiple-planet systems, we order systems based on the maximum occurrence among their individual planets. Consequently, the planets near the top of Table 1 are more frequent outcomes of planet formation and evolution than the planets near the bottom. We find that the occurrence-weighted mean period and insolation of the planets in our analysis sample are  $\bar{P} \approx 31$  days and  $\bar{F}_p \approx 27 F_{\oplus}$  respectively. In contrast, the mean period and insolation in our sample without occurrence weighting are  $\bar{P} \approx 21$  days and  $\bar{F}_p \approx 46 F_{\oplus}$  respectively.

### 3. ANALYSIS

We calculate occurrence-weighted median mass–radius, radius–mass, mass–density, and radius–density relations and their uncertainties using Monte Carlo simulations. On each iteration, we sample masses and radii for every planet in our analysis sample from the normal or asymmetric normal distributions representing the published uncertainties in masses and radii listed in Table 1. We assume that mass and radius inferences are uncorrelated. We next fit a cubic smoothing spline using the `smooth.spline` function with smoothing parameter  $s = 0.9$  as implemented in R (R Core Team 2020) while weighting each planet’s mass and radius point by the occurrence of that planet listed in Table 1. We use the smoothing spline to predict radius as a function of mass, mass as a function of radius, density as a function of mass, and density as a function of radius at 101 points evenly separated in the ranges  $0 M_{\oplus} \leq M_p \leq 20 M_{\oplus}$  or  $0 R_{\oplus} \leq R_p \leq 4 R_{\oplus}$  and save the result. We repeat this process 1,000 times to generate 1,000 occurrence-weighted mass–radius, radius–mass, mass–density, and radius–density relations. We illustrate the median occurrence-weighted mass–radius, radius–mass, mass–density, and radius–density relations and their uncertainties in Figures 2 and 3. We also include the full sample of 1,000 occurrence-weighted mass–radius, radius–mass, mass–density, and radius–density relations as machine-readable tables to enable others to make use of our occurrence-weighted relations. Characterizing our occurrence-weighted sample with  $\bar{F}_p \approx 27 F_{\oplus}$  as a single population with some dispersion as opposed to multiple populations is justified in this case because the small planet peak defining the so-called “Fulton Gap” disap-

<sup>1</sup> [https://www.pas.rochester.edu/~emamajek/EEM.dwarf\\_UBVIJHK\\_colors\\_Teff.txt](https://www.pas.rochester.edu/~emamajek/EEM.dwarf_UBVIJHK_colors_Teff.txt)

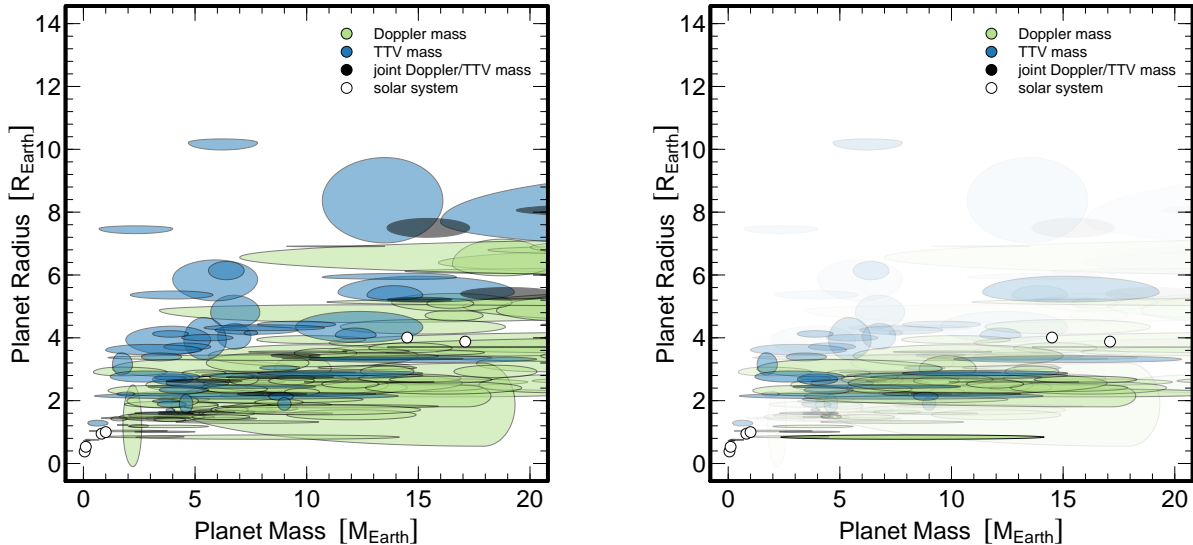


**Figure 1.** Inferred masses and radii for planets with masses consistent with  $M_p \leq 20 M_\oplus$  at the  $3\text{-}\sigma$  level orbiting solar-type stars listed in Table 1. Each ellipse is centered on a planet’s inferred mass and radius and represents the  $1\text{-}\sigma$  uncertainty in the mass and radius of the planet assuming no covariance between mass and radius inferences. We plot masses inferred by the Doppler effect in blue, by transit-timing variations (TTVs) in green, and by joint Doppler/TTV analyses in black. We plot solar system planets as open circles. Left: opacity of each ellipse independent of planet occurrence. Right: opacity of each ellipse proportional to the [Hsu et al. \(2019\)](#) occurrence of planets with the period and radius of the planet represented by the ellipse. The right panel provides a less-biased view of the Galaxy’s planet population than the heavily biased view illustrated in the left panel. Among the analysis sample of planets orbiting solar-type stars with currently available mass inferences, the most common planets have  $2 R_\oplus \lesssim R_p \lesssim 3 R_\oplus$  over the mass range  $1 M_\oplus \lesssim M_p \lesssim 20 M_\oplus$ .

pears at planet insolation  $F_p \lesssim 30 F_\oplus$  (e.g., [Fulton et al. 2017](#)).

We compare our occurrence-weighted relations to theoretical models for both solid planets and rocky planets with significant H/He atmospheres. For solid planets, we use models from [Zeng et al. \(2019\)](#). For rocky planets with significant H/He atmospheres, we interpolate the grid of models presented in [Lopez & Fortney \(2014\)](#) to calculate radii as a function of mass and H/He atmosphere mass fraction for a 5 Gyr old planet population experiencing the occurrence-weighted mean insolation of our sample  $\bar{F}_p = 27 F_\oplus$ . We find that our occurrence-weighted mass–radius relation demands that planets with  $M_p \approx 2.3 M_\oplus$  must have at least 1% of their masses in H/He atmospheres. Our occurrence-weighted mass–radius relation indicates that in the range  $0 M_\oplus \leq M_p \leq 7 M_\oplus$ , the fractional mass in a planet’s H/He atmosphere increases with mass from 1% at  $M_p \approx 2 M_\oplus$  to more than 3% at  $M_p \approx 7 M_\oplus$ . Our occurrence-weighted mass–radius relation provides no reason to believe that the fractional mass in a planet’s H/He atmosphere scales with mass in the range  $7 M_\oplus \lesssim M_p \lesssim 20 M_\oplus$ . Indeed, in the mass range  $9 M_\oplus \lesssim M_p \lesssim 20 M_\oplus$  the occurrence-weighted mass–radius relation is consistent with both rocky planets with H/He atmospheres and planets made entirely of water without H/He atmo-

spheres. In the mass range corresponding to the ice giants Uranus and Neptune in our own solar system ( $15 M_\oplus \lesssim M_p \lesssim 20 M_\oplus$ ), the occurrence-weighted median planet has at most 5% of its mass in a H/He atmosphere. This is in contrast to Uranus and Neptune that have at least 10% of their masses in H/He atmospheres (e.g., [Podolak et al. 2019](#); [Helled & Fortney 2020](#)).

Our occurrence-weighted radius–mass relation requires that planets with  $R_p \gtrsim 2.7 R_\oplus$  must have some H/He and planets with  $R_p \gtrsim 2.8 R_\oplus$  must have at least 3% of their masses in H/He atmospheres. Below these critical radii, the occurrence-weighted radius–mass relation cannot exclude planets made entirely of water without H/He atmospheres. The flat occurrence-weighted radius–mass relation in the range  $3 R_\oplus \lesssim R_p \lesssim 4 R_\oplus$  implies that planets in that interval grow in radius by accreting H/He without adding much mass. This growth in radius at constant mass also suggests a typical core mass  $M_c \approx 10 M_\oplus$ .

Our occurrence-weighted mass–density and radius–density relations are much less precise because density estimates are affected by both mass and radius uncertainties. Nevertheless, the occurrence-weighted median  $M_p \approx 1 M_\oplus$  planet is less dense than the terrestrial planets in our solar system and the occurrence-weighted median planet in the range  $15 M_\oplus \lesssim M_p \lesssim 20 M_\oplus$  is



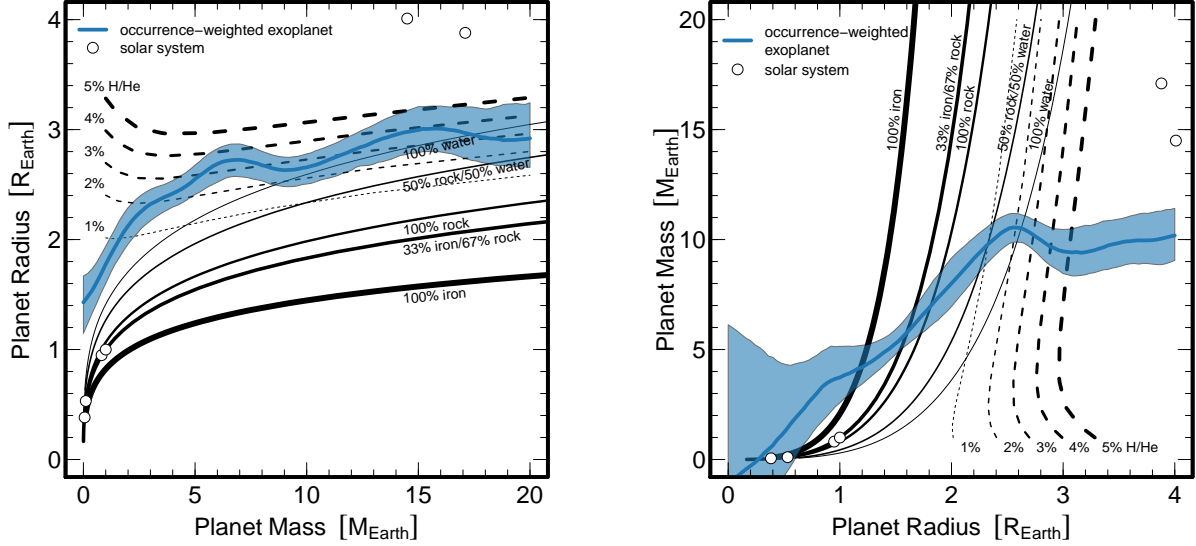


**Figure 2.** Mass–radius and radius–mass relations resulting from occurrence-weighted smoothing spline fits to individual iterations of a Monte Carlo simulation sampling planet masses and radii from their uncertainty distributions as described in Table 1. The solid dark blue line corresponds to the median occurrence-weighted smoothing spline radius or mass at given mass or radius. The light blue region spans the 16th to 84th percentiles of the occurrence-weighted smoothing spline radius or mass at given mass or radius. We plot solar system planets as open circles. We plot as solid black lines theoretical models from Zeng et al. (2019) for planets without H/He atmospheres and as dashed black lines theoretical models from Lopez & Fortney (2014) for planets with significant H/He atmospheres. For the Lopez & Fortney (2014) models we assume an age of 5 Gyr and insolation  $F_p = 27 F_\oplus$  equal to the occurrence-weighted mean insolation of our sample. Left: occurrence-weighted exoplanet radius given mass. Among the sample of planets with currently available mass inferences, the occurrence-weighted median planet at  $M_p \approx 2.3 M_\oplus$  must have at least 1% of its mass in a H/He atmosphere to explain its radius. In contrast to Uranus and Neptune that have at least 10% of their masses in H/He atmospheres, in the range  $15 M_\oplus \lesssim M_p \lesssim 20 M_\oplus$  the occurrence-weighted median planet has at most 5% of its mass in a H/He atmosphere. Right: occurrence-weighted exoplanet mass given radius. Among the sample of planets with currently available mass inferences, the occurrence-weighted median planet with  $R_p \gtrsim 2.7 R_\oplus$  must have some H/He and the occurrence-weighted median planet with  $R_p \gtrsim 2.8 R_\oplus$  must have at least 3% of its mass in a H/He atmosphere. The flat occurrence-weighted radius–mass relation in the range  $3 R_\oplus \lesssim R_p \lesssim 4 R_\oplus$  shows that planets in that interval grow in radius by accreting H/He and have a typical core mass  $M_c \approx 10 M_\oplus$ .

more dense than the ice giants Uranus and Neptune. The occurrence-weighted radius–density relation confirms that planets with  $R_p \gtrsim 2.7 R_\oplus$  must have some H/He and planets with  $R_p \gtrsim 2.8 R_\oplus$  must have at least 3% of their masses in H/He atmospheres.

Armitage (2010) derived the minimum planet mass necessary for a core to maintain an isothermal H/He envelope with a small but non-negligible mass fraction  $\epsilon$

$$M_p \gtrsim \left( \frac{3}{4\pi\rho_m} \right)^{1/2} \left( \frac{c_s^2}{G} \right)^{3/2} \left[ \ln \left( \frac{\epsilon\rho_m}{\rho_0} \right) \right]^{3/2}, \quad (1)$$

where  $\rho_m$  is the density of the core,  $c_s$  and  $\rho_0$  are the gas sound speed and density in the midplane of the core’s parent protoplanetary disk, and  $G$  is the gravitational constant. We use the analytic protoplanetary disk models of Bell et al. (1997) to evaluate if our observation that the occurrence-weighted median planet with  $M_p \approx 2.3 M_\oplus$  must have at least 1% of its mass in a H/He envelope is consistent with the expected out-

come of the planet formation process for a planet with  $M_p = 2.3 M_\oplus$ . We assume a mean molecular weight  $\mu = 2.3$  appropriate for molecular hydrogen and helium in the solar ratio. We assume a  $M_* = 1 M_\odot$  host star and calculate disk structure as a function of Shakura-Sunyaev  $\alpha$  parameter and mass accretion rate  $\dot{M}$ . We plot these disk models in Figure 4.

We use these disk models to estimate with Equation (1) the mass necessary for a planet with density  $\rho_m = 5.5 \text{ g cm}^{-3}$  consistent with the bulk density of the Earth to maintain an isothermal H/He envelope with mass fraction  $\epsilon = 0.01$ . We plot the inferred minimum mass as a function of Shakura-Sunyaev  $\alpha$  parameter and mass accretion rate in Figure 5. We find that for Shakura-Sunyaev  $\alpha$  parameter in the range  $10^{-4} \leq \alpha \leq 10^{-2}$  and mass accretion rate in the range  $10^{-9} M_\odot \text{ yr}^{-1} \leq \dot{M} \leq 10^{-7} M_\odot \text{ yr}^{-1}$ , planets with  $M_p \gtrsim 1.5 M_\oplus$  should be able to maintain isothermal H/He envelopes. This theoretical expectation is fully consistent with our observation that the occurrence-

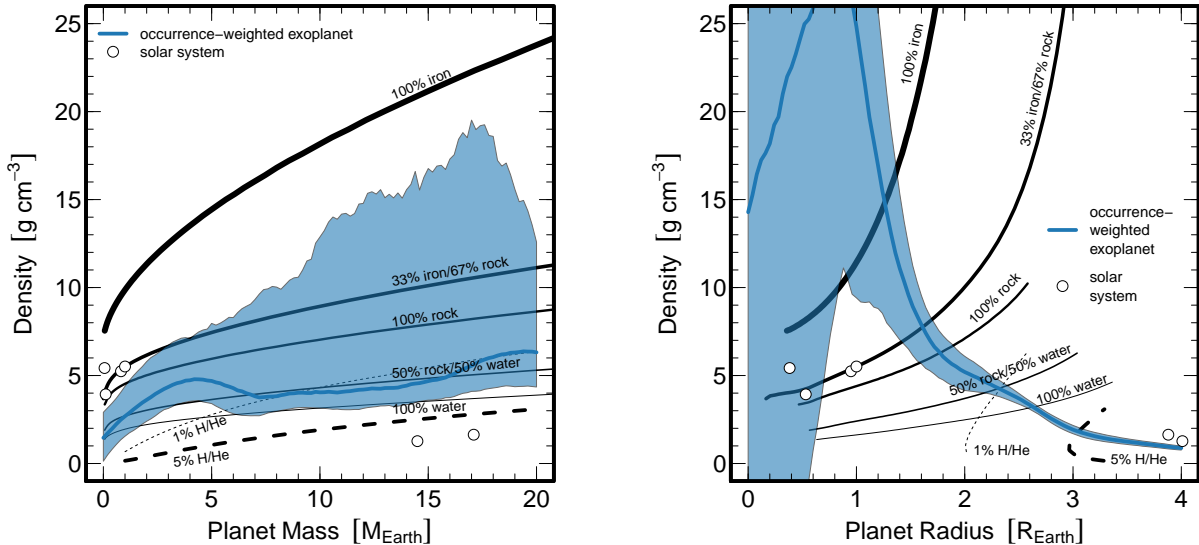


**Figure 3.** Mass–density and radius–density relations resulting from occurrence-weighted smoothing spline fits to individual iterations of a Monte Carlo simulation sampling planet masses and radii from their uncertainty distributions as described in Table 1. The solid dark blue line corresponds to the median occurrence-weighted smoothing spline density at given mass or radius. The light blue region spans the 16th to 84th percentiles of the occurrence-weighted smoothing spline density at given mass or radius. We plot solar system planets as open circles. We plot theoretical models from Zeng et al. (2019) for planets without H/He atmospheres as black lines and theoretical models from Lopez & Fortney (2014) for planets with significant H/He atmospheres as dashed lines. For the Lopez & Fortney (2014) models we assume an age of 5 Gyr and insolation  $F_p = 27 F_\oplus$  equal to the occurrence-weighted mean insolation of our sample. Left: occurrence-weighted exoplanet density given mass. Among the sample of planets with currently available mass inferences, the occurrence-weighted median planet is less dense than the terrestrial planets but denser than the ice giants in our solar system. Right: occurrence-weighted exoplanet density given radius. Among the sample of planets with currently available mass inferences, the occurrence-weighted median planet with  $R_p \gtrsim 2.7 R_\oplus$  must have some H/He and the occurrence-weighted median planet with  $R_p \gtrsim 2.8 R_\oplus$  must have at least 3% of its mass in a H/He atmosphere.

weighted median planet with  $M_p \approx 2.3 M_\oplus$  must have at least 1% of its mass in a H/He atmosphere to simultaneously explain its mass and radius. While this is an idealized theoretical model, similar results are found in state-of-the-art exoplanet population synthesis models with much more detailed and comprehensive treatments of the physics of planet formation (e.g., Emsenhuber et al. 2020a,b).

#### 4. DISCUSSION

We compare our occurrence-weighted mass–radius and radius–mass relations to published mass–radius and radius–mass relations without occurrence weighting in Figures 6 and 7. When compared to the mass–radius relations in the literature, our occurrence-weighted mass–radius relation suggests larger-radius  $M_p \approx 1 M_\oplus$  planets and smaller-radius  $M_p \approx 20 M_\oplus$  planets. Our occurrence-weighted radius–mass relation is consistent with most published radius–mass relations.

We find that the occurrence-weighted median planets discovered so far by transit surveys have at least 1% of their mass in H/He atmospheres at  $M_p \approx 2.3 M_\oplus$ . The fraction of mass in H/He atmospheres increases from 1%

at  $M_p \approx 2 M_\oplus$  to at least 3% at  $M_p \approx 7 M_\oplus$  then stays consistent with 3% up to  $M_p \approx 20 M_\oplus$ . The occurrence-weighted median planet is also consistent with a 100% water composition in the range  $9 M_\oplus \lesssim M_p \lesssim 20 M_\oplus$ . The occurrence-weighted median planets discovered so far by transit surveys are at constant mass less dense than the terrestrial planets and more dense than the ice giants.

A planet with a significant H/He atmosphere must have formed before the dissipation of its parent protoplanetary disk. Observations of the fraction of stars in young clusters with disks or accretion from disks as a function of cluster age indicate that disk dissipation occurs on a characteristic timescale  $t_{\text{disk}} \approx 3$  Myr (e.g., Haisch et al. 2001; Cieza et al. 2007; Fedele et al. 2010). The short characteristic disk dissipation time therefore requires the formation of the occurrence-weighted median terrestrial-mass planets early in their host systems’ evolution. This early formation is in contrast to the Earth, which only reached  $M_p \approx 0.6 M_\oplus$  in the first 4.5 Myr after the formation of calcium & aluminum rich inclusions (CAIs) at the dawn of the solar system and

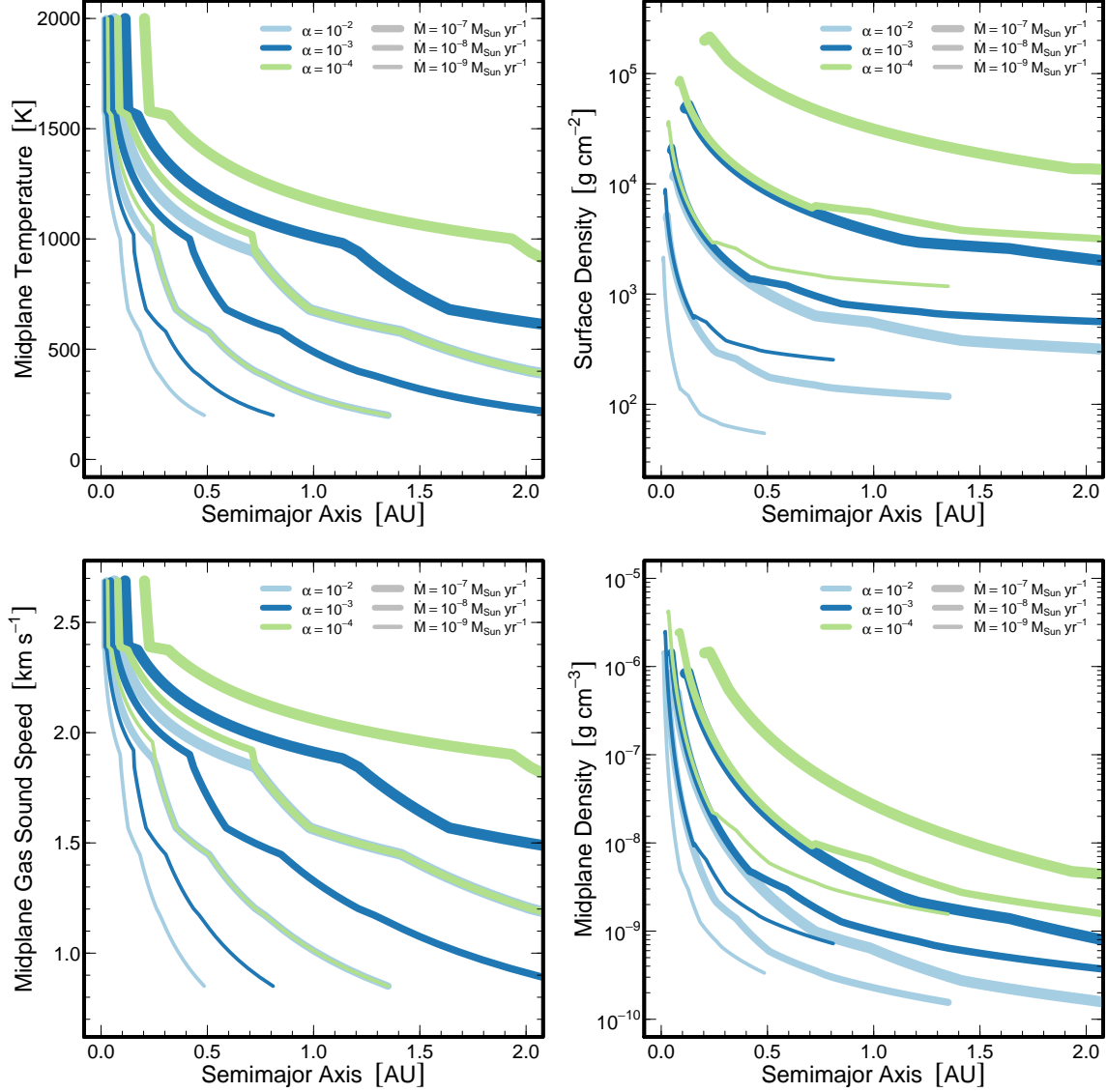


**Figure 4.** Protoplanetary disk midplane temperature  $T_{\text{disk}}$ , surface density  $\Sigma$ , midplane gas sound speed  $c_s$ , and midplane density  $\rho_0$  predicted by the analytic model of Bell et al. (1997) as a function of Shakura-Sunyaev  $\alpha$  parameter and mass accretion rate.

did not finish forming its core for an additional 40 Myr (e.g., Kleine et al. 2009; Lammer et al. 2021). It may be that the solar system lacks short-period super-Earth or mini-Neptune planets like those found by Kepler because of differences in the timescale for planetary embryos to reach  $M_p \approx 1 M_\oplus$ . In planetary systems with short-period super-Earth or mini-Neptune planets, planetary embryos must have grown to  $M_p \gtrsim 1 M_\oplus$  before the gas-rich phase of their parent protoplanetary disks’ evolution ended. On the other hand, it appears that the planetary embryos in the inner solar system that would grow into the terrestrial planets did not reach  $M_p \approx 1 M_\oplus$  during the gas-rich phase of the protosolar nebula’s evolution even though models suggest that oligarchic growth at 1

AU should have been complete 1 Myr after the formation of planetesimals (e.g., Kokubo & Ida 2000).

The fact that the occurrence-weighted median planet has no more than a few percent of its mass in a H/He envelope over the mass range  $2 M_\oplus \lesssim M_p \lesssim 8 M_\oplus$  requires a core mass distribution extending from  $M_c = 2 M_\oplus$  to at least  $M_c = 8 M_\oplus$ . Parameterized models of photoevaporative mass loss reach the same conclusion in a very different way (e.g., Rogers & Owen 2021), supporting the robustness of this inference. Similar core mass distributions can be realized by planet formation in gas-poor protoplanetary disks (e.g., Lee & Connors 2021), though a mixture of rocky and icy cores may be necessary simultaneously explain both low- and high-

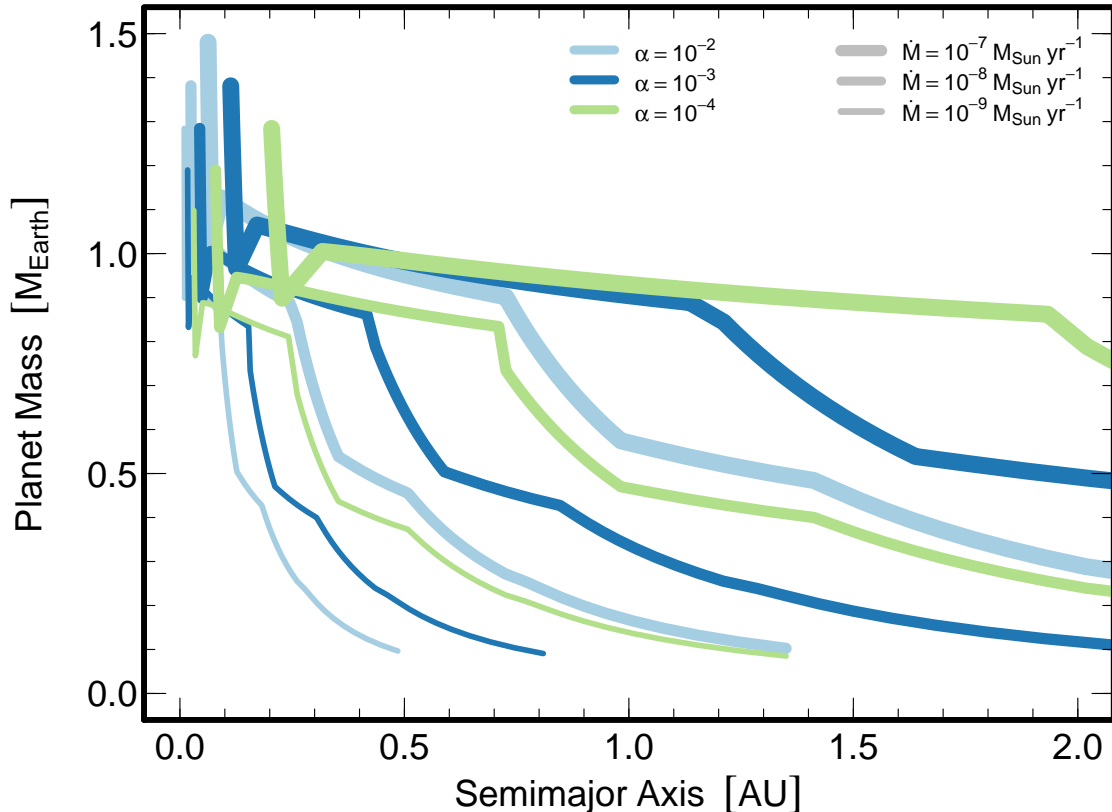


**Figure 5.** Mass above which an embedded protoplanet can be expected to retain an isothermal H/He envelope equal to 1% of its total mass accreted from its parent protoplanetary disk assuming the analytic disk models of Bell et al. (1997) and an Earth-composition density. The predictions of this analytic disk model are in accord with our observation that the occurrence-weighted median planet at  $M_p \approx 2.3 M_\oplus$  has at least 1% if its mass in a H/He atmosphere.

mass extremes of the distribution (e.g., Venturini et al. 2020a,b).

The existence of a 1% H/He atmosphere around a planet with  $M_p \approx 2 M_\oplus$  orbiting a solar-type star with  $F_p \approx 27 F_\oplus$  can be used to constrain models of atmospheric escape. Lopez & Fortney (2013) simulated the photoevaporation of low mean molecular weight atmospheres of low-mass planets by stellar extreme ultraviolet (EUV) irradiation as a function core mass, atmosphere mass, system age, and efficiency of mass loss. According to those simulations, our observation of a 1% H/He atmospheres around a planet with  $M_p \approx 2 M_\oplus$  several Gyr old can only be accommodated if the fraction of incident EUV flux converted into work is relatively low  $\epsilon_{\text{evap}} \sim 0.01$ . This is an order of magnitude lower than the value  $\epsilon_{\text{evap}} \sim 0.1$  inferred from detailed models of EUV-driven mass loss from hot Jupiters, short-period Neptune-mass planets, and the Kepler-11 and Kepler-36 systems (e.g., Murray-Clay et al. 2009; Owen & Jackson 2012; Lopez et al. 2012; Lopez & Fortney 2013). While it has usually been assumed that a

solar-type star’s X-ray and EUV luminosities decay at the same rate, King & Wheatley (2021) have recently suggested that EUV emission falls off much more slowly than X-ray emission. As a consequence, a planet experiences most of its total total X-ray and EUV irradiation between 100 Myr and 10 Gyr after its formation. This extended irradiation may be supported by the observational results of David et al. (2021) and could complicate the interpretation of the existence of 1% H/He atmosphere around a planet with  $M_p \approx 2 M_\oplus$  orbiting a solar-type star in the context of the Lopez & Fortney (2013) model.

The alternative core-driven mass loss model proposed by Ginzburg et al. (2016) can only accommodate the existence of 1% H/He atmospheres around planets with  $M_p \approx 2 M_\oplus$  if those planets have low equilibrium temperatures and therefore compact atmospheres. At the occurrence-weighted average semimajor axis  $\bar{a} = 0.19$  AU of our analysis sample, an equilibrium temperature that low can only be achieved if the occurrence-weighted median terrestrial-mass planets have Bond



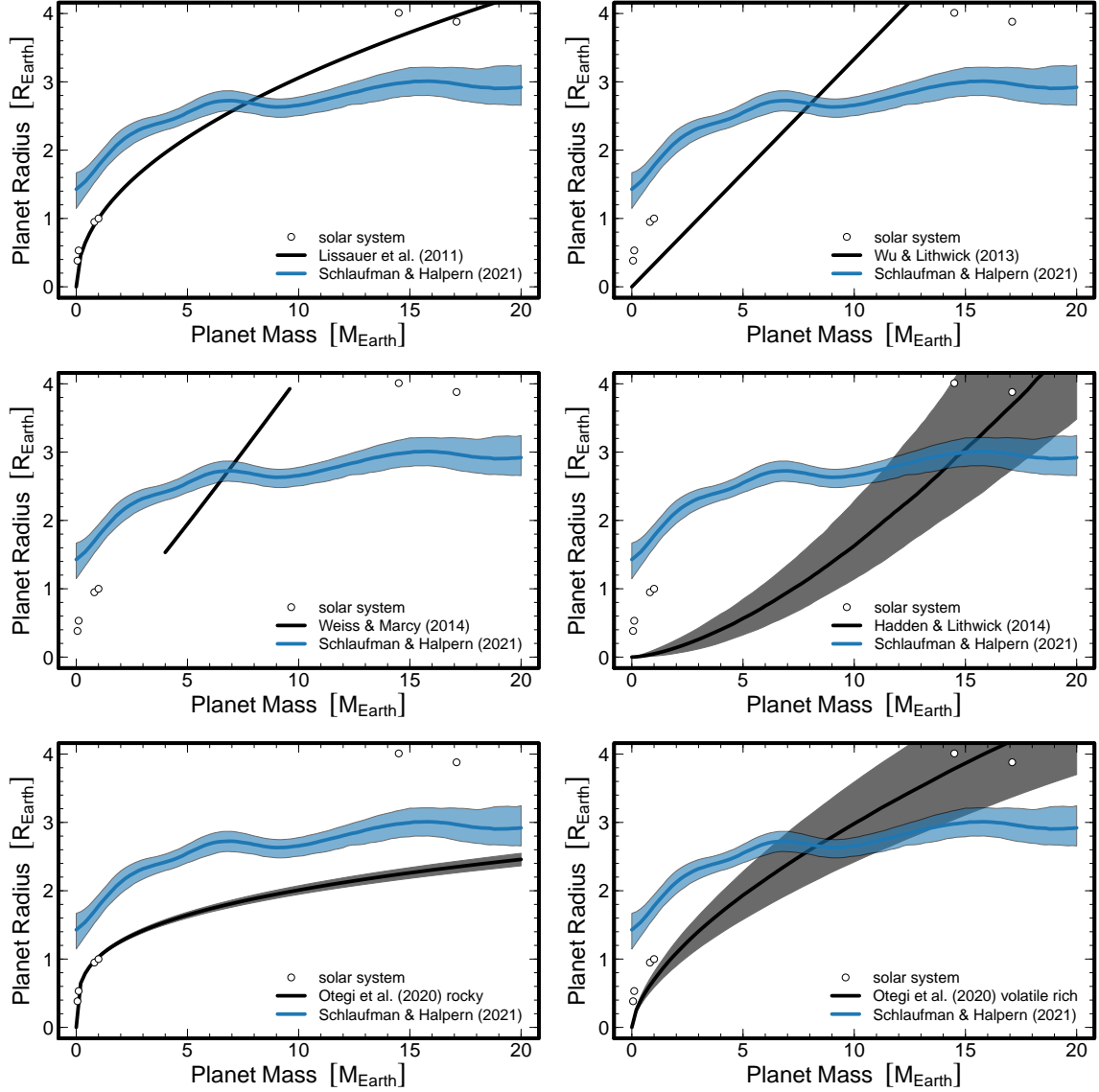


**Figure 6.** Comparison of our occurrence-weighted mass–radius with previously published relations without occurrence weighting. We plot the central value of each relation with a line and indicate its  $1\text{-}\sigma$  uncertainty if available with a shaded polygon. Our occurrence-weighted mass–radius relation indicates that planets with  $M_p \approx 1 M_\oplus$  are larger and  $M_p \approx 20 M_\oplus$  are smaller than previously found.

albedos  $A_B \gtrsim 0.95$ . Regardless of the mass loss mechanism, we predict that more planets with  $M_p \sim 1 M_\oplus$  and  $R_p \approx 2 R_\oplus$  orbiting solar-type stars will be discovered and characterized as mass and radius inferences become possible for low-mass planets with  $P \gtrsim 40$  days,  $a \gtrsim 0.25$  AU, and  $F_p \lesssim 20 F_\oplus$  (e.g., Alessi et al. 2020; Neil & Rogers 2020).

The occurrence-weighted median planets in the mass range  $15 M_\oplus \lesssim M_p \lesssim 20 M_\oplus$  are massive enough to avoid the loss of their atmospheres due to EUV or core-driven mass loss, so the observation that they have no more than than 5% of their masses in H/He atmospheres constrains their formation. Hot disks produce small

H/He atmospheres at constant core mass (Ikoma & Hori 2012). Short-lived disks and large opacities (possibly maintained by atmospheric recycling with disk gas) may also keep H/He mass fractions low (e.g., Lee & Chiang 2015; Ginzburg et al. 2016; Ogihara et al. 2020; Ormel et al. 2021). Exoplanet population synthesis calculations can produce Neptune-mass planets with small H/He atmospheres if collisions with other planet mass bodies occur before the parent protoplanetary disk is completely dissipated (e.g., Emsenhuber et al. 2020a,b; Schlecker et al. 2021). These collisions could be a ubiquitous feature of planet formation as systems of planets driven into mean-motion resonances by disk migration may experi-

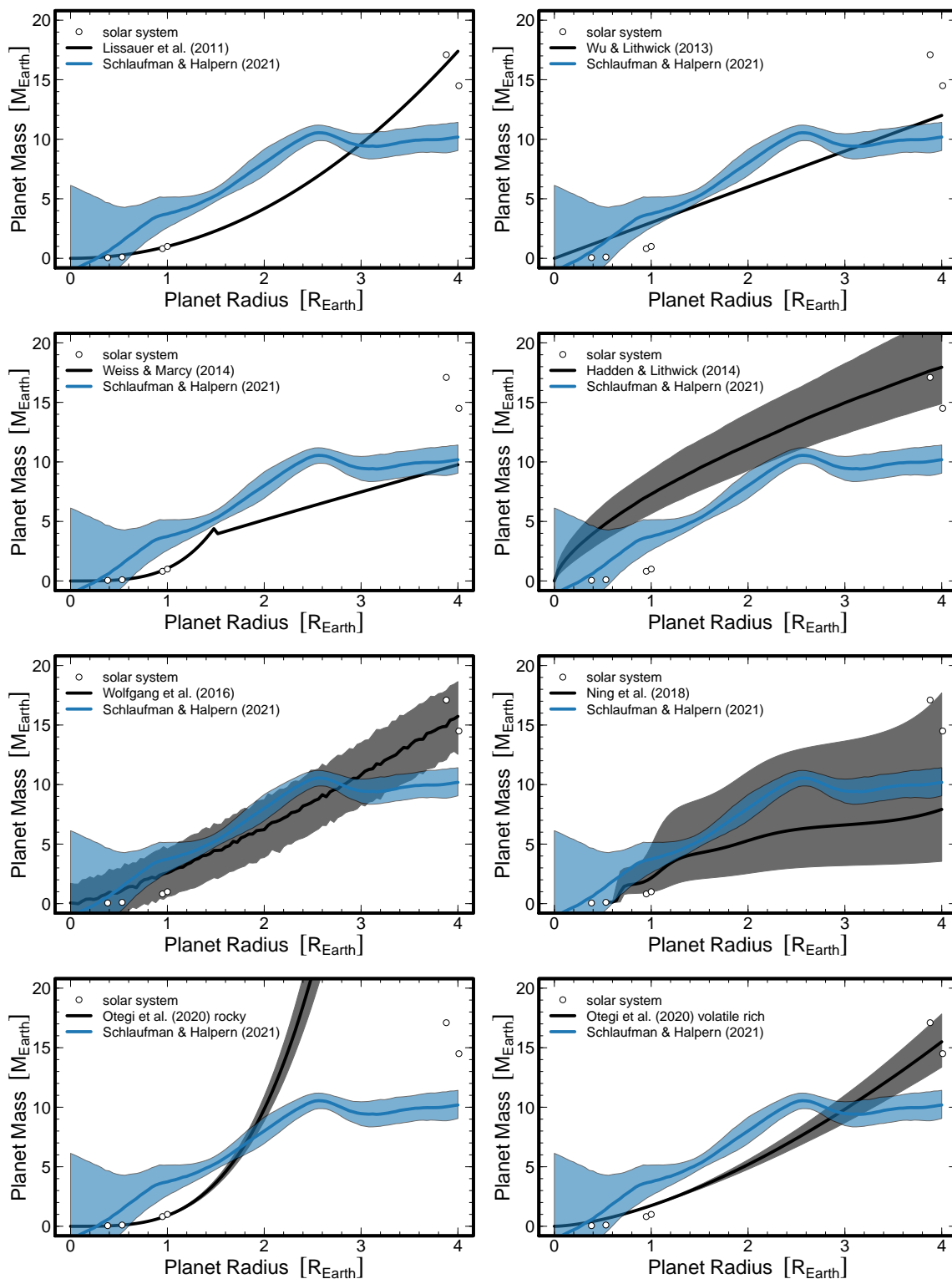


**Figure 7.** Comparison of our occurrence-weighted mass–radius and radius–mass relations with previously published relations without occurrence weighting. We plot the central value of each relation with a line and indicate its 1- $\sigma$  uncertainty if available with a shaded polygon. Our occurrence-weighted radius–mass relation is consistent with most relations in the literature.

ence dynamical instabilities and giant impacts as their parent protoplanetary disk dissipates (e.g., Izidoro et al. 2017; Ogihara et al. 2020).

The left-hand panel of Figure 2 further shows that the occurrence-weighted median planet in the mass range  $10 M_{\oplus} \lesssim M_p \lesssim 20 M_{\oplus}$  is core dominated, either icy or rocky with a small H/He envelope. The right-hand panel of Figure 2 shows that the occurrence-weighted median planet in the radius range  $3 R_{\oplus} \lesssim R_p \lesssim 4 R_{\oplus}$  grows in radius but not mass by adding mass in a H/He atmosphere. These two observations suggest that the occurrence-weighted median planets with  $2 R_{\oplus} \lesssim R_p \lesssim 3 R_{\oplus}$  have a broad range of core masses, while the occurrence-weighted median planets with  $R_p \gtrsim 3 R_{\oplus}$  have cores with  $M_c \approx 10 M_{\oplus}$ . This inference is in accord with the classical threshold of  $M_c \approx 10 M_{\oplus}$  for runaway envelope accretion and giant planet formation (e.g., Pollack et al. 1996; Hubickyj et al. 2005). We therefore argue that the occurrence-weighted median planets in the mass range  $15 M_{\oplus} \lesssim M_p \lesssim 20 M_{\oplus}$  formed (1) in hotter parts of their parent protoplanetary disks than Uranus and Neptune, (2) shortly before the dissipation of their parent protoplanetary disks, and/or (3) after experiencing collisions with other planet-mass bodies as their parent protoplanetary disk was dissipated. We favor the collision hypothesis for planets with  $10 M_{\oplus} \lesssim M_p \lesssim 20 M_{\oplus}$  and  $2 R_{\oplus} \lesssim R_p \lesssim 3 R_{\oplus}$ .

While our occurrence-weighted mass–radius, radius–mass, mass–density, and radius–density relations mitigate some of the observational biases in previous studies, they do not completely eliminate them. If at  $P \lesssim 1$  yr Earth-composition planets with  $M_p \approx 2.3 M_{\oplus}$  and  $R_p \approx 1.3 R_{\oplus}$  are a more common outcome of the planet formation process than H/He atmosphere planets with  $M_p \approx 2.3 M_{\oplus}$  and  $R_p \approx 2.2 R_{\oplus}$ , then the former population would be underrepresented even in data from the Kepler prime mission due to the strong planet radius dependence of the number of detections in a photon-noise limited transit survey. Though the two populations would have identical Doppler semi-amplitudes, the population of  $M_p \approx 2.3 M_{\oplus}$  and  $R_p \approx 1.3 R_{\oplus}$  planets would often evade detection and therefore never be subject to follow-up Doppler observations. TTV-based mass inferences for the  $M_p \approx 2.3 M_{\oplus}$  and  $R_p \approx 1.3 R_{\oplus}$  population would be more difficult as well. The net result is that there could be a population of Earth-composition,  $M_p \approx 2.3 M_{\oplus}$ , and  $R_p \approx 1.3 R_{\oplus}$  planets that finished forming after the end of the gas-rich phase of their parent protoplanetary disks’ evolution and is a more common outcome of planet formation than the occurrence-weighted median planets described in this paper. Even if this so, then the conclusion that H/He atmosphere plan-

ets with  $M_p \approx 2.3 M_{\oplus}$  and  $R_p \approx 2.2 R_{\oplus}$  form before the end of the gas-rich phase of their parent protoplanetary disks’ evolution is unchanged. The existence of a largely unobserved population of Earth-composition,  $M_p \approx 2.3 M_{\oplus}$ , and  $R_p \approx 1.3 R_{\oplus}$  planets at  $P \gtrsim \bar{P} = 31$  days does not affect our inferences about photoevaporation, core-driven mass loss, or the structure & formation of the occurrence-weighted median Neptune-mass planets.

## 5. CONCLUSION

We derive occurrence-weighted mass–radius, radius–mass, mass–density, and radius–density relations for the exoplanets discovered so far by transit surveys. These occurrence-weighted relations mitigate some of the biases of the transit technique and the Doppler/TTV mass inference methods. They should provide a less-biased view of the typical outcome of the planet formation process in the solar neighborhood than mass–radius relations that have not accounted for planet occurrence. We find that the occurrence-weighted median planet with  $M_p \approx 2.3 M_{\oplus}$  must have at least 1% of its mass in a H/He atmosphere. The fraction of mass in the occurrence-weighted median planet’s H/He atmosphere increases from 1% at  $M_p \approx 2 M_{\oplus}$  to at least 3% at  $M_p \approx 7 M_{\oplus}$ . Our observation that the occurrence-weighted median planet has only a few percent of its mass in a H/He envelope implies a core mass distribution extending from  $M_c = 2 M_{\oplus}$  to at least  $M_c = 8 M_{\oplus}$ . There is no discernible increase in H/He atmosphere mass fraction in the range  $7 M_{\oplus} \lesssim M_p \lesssim 20 M_{\oplus}$  and 100% water compositions cannot be rejected for planets with  $9 M_{\oplus} \lesssim M_p \lesssim 20 M_{\oplus}$ . The occurrence-weighted median  $M_p \approx 1 M_{\oplus}$  planet is less dense than the terrestrial planets in our solar system, but the occurrence-weighted median planet with  $15 M_{\oplus} \lesssim M_p \lesssim 20 M_{\oplus}$  is denser than the ice giants. The accretion of a 1% H/He envelope by a planet with  $M_p \approx 2 M_{\oplus}$  is the expected outcome of the core-accretion process in protoplanetary disks with a range of Shakura-Sunyaev  $\alpha$  parameters and mass accretion rates. The retention of that atmosphere over Gyr timescales indicates that EUV-driven photoevaporation atmosphere loss is less efficient than usually assumed and/or that core-driven atmosphere loss is avoided because of large Bond albedos. While Uranus and Neptune have about 10% of their masses in H/He atmospheres, the observation that the occurrence-weighted median planet with  $15 M_{\oplus} \lesssim M_p \lesssim 20 M_{\oplus}$  has at most 5% of its mass in a H/He atmosphere implies that it formed in a hotter or shorter-lived part of its parent protoplanetary disk than Uranus and Neptune. It could also indicate that giant impacts during

disk dissipation are a common stage of the formation of short-period planets with  $10 M_{\oplus} \lesssim M_p \lesssim 20 M_{\oplus}$ , especially those in the radius range  $2 R_{\oplus} \lesssim R_p \lesssim 3 R_{\oplus}$ .

We are grateful to the anonymous referee for an insightful review of our paper and for suggestions that significantly improved our analyses. We thank Bertram Bitsch, Eric Ford, Dan Fabrycky, Eve Lee, Eric Lopez, Christoph Mordasini, and Leslie Rogers for helpful comments. This research has made use of the NASA Exoplanet Archive, which is operated by the California Institute of Technology, under contract with the National Aeronautics and Space Administration under the Exoplanet Exploration Program. This research has made use of the SIMBAD database, operated at CDS, Strasbourg, France (Wenger et al. 2000). This work has made use of data from the European Space Agency (ESA) mission *Gaia* (<https://www.cosmos.esa.int/gaia>), processed by the *Gaia* Data Processing and Analysis Consortium (DPAC, <https://www.cosmos.esa.int/web/gaia/dpac/consortium>). Funding for the DPAC has been provided by national institutions, in particular the institutions participating in the *Gaia* Multilateral Agreement. This research has made use of the VizieR catalogue access tool, CDS, Strasbourg, France (DOI: 10.26093/cds/vizieR). The original description of the VizieR service was published in 2000, A&AS 143, 23 (Ochsenbein et al. 2000). This research has made use of NASA’s Astrophysics Data System.

*Facilities:* Exoplanet Archive

*Software:* R (R Core Team 2020), TOPCAT (Taylor 2005)

## REFERENCES

- Adams, E. R., Seager, S., & Elkins-Tanton, L. 2008, *ApJ*, 673, 1160, doi: [10.1086/524925](https://doi.org/10.1086/524925)
- Adams, E. R., Jackson, B., Endl, M., et al. 2017, *AJ*, 153, 82, doi: [10.3847/1538-3881/153/2/82](https://doi.org/10.3847/1538-3881/153/2/82)
- Akeson, R. L., Chen, X., Ciardi, D., et al. 2013, *PASP*, 125, 989, doi: [10.1086/672273](https://doi.org/10.1086/672273)
- Alessi, M., Inglis, J., & Pudritz, R. E. 2020, *MNRAS*, 497, 4814, doi: [10.1093/mnras/staa2087](https://doi.org/10.1093/mnras/staa2087)
- Alonso, R., Moutou, C., Endl, M., et al. 2014, *A&A*, 567, A112, doi: [10.1051/0004-6361/201118662](https://doi.org/10.1051/0004-6361/201118662)
- Arenou, F., Luri, X., Babusiaux, C., et al. 2018, *A&A*, 616, A17, doi: [10.1051/0004-6361/201833234](https://doi.org/10.1051/0004-6361/201833234)
- Armitage, P. J. 2010, *Astrophysics of Planet Formation* (Cambridge: Cambridge University Press)
- Bailer-Jones, C. A. L., Rybizki, J., Fouesneau, M., Mantelet, G., & Andrae, R. 2018, *AJ*, 156, 58, doi: [10.3847/1538-3881/aacb21](https://doi.org/10.3847/1538-3881/aacb21)
- Ballard, S., Fabrycky, D., Fressin, F., et al. 2011, *ApJ*, 743, 200, doi: [10.1088/0004-637X/743/2/200](https://doi.org/10.1088/0004-637X/743/2/200)
- Barragán, O., Grziwa, S., Gandolfi, D., et al. 2016, *AJ*, 152, 193, doi: [10.3847/0004-6256/152/6/193](https://doi.org/10.3847/0004-6256/152/6/193)
- Barros, S. C. C., Gosselin, H., Lillo-Box, J., et al. 2017, *A&A*, 608, A25, doi: [10.1051/0004-6361/201731276](https://doi.org/10.1051/0004-6361/201731276)
- Batalha, N. M., Borucki, W. J., Bryson, S. T., et al. 2011, *ApJ*, 729, 27, doi: [10.1088/0004-637X/729/1/27](https://doi.org/10.1088/0004-637X/729/1/27)
- Becker, J. C., Vanderburg, A., Adams, F. C., Rappaport, S. A., & Schwengel, H. M. 2015, *ApJL*, 812, L18, doi: [10.1088/2041-8205/812/2/L18](https://doi.org/10.1088/2041-8205/812/2/L18)
- Bell, K. R., Cassen, P. M., Klahr, H. H., & Henning, T. 1997, *ApJ*, 486, 372, doi: [10.1086/304514](https://doi.org/10.1086/304514)
- Berger, T. A., Huber, D., van Saders, J. L., et al. 2020, *AJ*, 159, 280, doi: [10.3847/1538-3881/159/6/280](https://doi.org/10.3847/1538-3881/159/6/280)
- Bonomo, A. S., Zeng, L., Damasso, M., et al. 2019, *Nature Astronomy*, 3, 416, doi: [10.1038/s41550-018-0684-9](https://doi.org/10.1038/s41550-018-0684-9)
- Borucki, W. J., Koch, D. G., Brown, T. M., et al. 2010, *ApJL*, 713, L126, doi: [10.1088/2041-8205/713/2/L126](https://doi.org/10.1088/2041-8205/713/2/L126)
- Bouffeur, R. C., Emilio, M., Janot-Pacheco, E., et al. 2018, *MNRAS*, 473, 710, doi: [10.1093/mnras/stx2187](https://doi.org/10.1093/mnras/stx2187)
- Brahm, R., Hartman, J. D., Jordán, A., et al. 2018, *AJ*, 155, 112, doi: [10.3847/1538-3881/aaa898](https://doi.org/10.3847/1538-3881/aaa898)
- Brewer, J. M., & Fischer, D. A. 2018, *ApJS*, 237, 38, doi: [10.3847/1538-4365/aad501](https://doi.org/10.3847/1538-4365/aad501)
- Bruno, G., Almenara, J. M., Barros, S. C. C., et al. 2015, *A&A*, 573, A124, doi: [10.1051/0004-6361/201424591](https://doi.org/10.1051/0004-6361/201424591)
- Buchhave, L. A., Dressing, C. D., Dumusque, X., et al. 2016, *AJ*, 152, 160, doi: [10.3847/0004-6256/152/6/160](https://doi.org/10.3847/0004-6256/152/6/160)
- Burt, J. A., Nielsen, L. D., Quinn, S. N., et al. 2020, *AJ*, 160, 153, doi: [10.3847/1538-3881/abac0c](https://doi.org/10.3847/1538-3881/abac0c)
- Campante, T. L., Barclay, T., Swift, J. J., et al. 2015, *ApJ*, 799, 170, doi: [10.1088/0004-637X/799/2/170](https://doi.org/10.1088/0004-637X/799/2/170)
- Carleo, I., Gandolfi, D., Barragán, O., et al. 2020, *AJ*, 160, 114, doi: [10.3847/1538-3881/aba124](https://doi.org/10.3847/1538-3881/aba124)
- Carter, J. A., Agol, E., Chaplin, W. J., et al. 2012, *Science*, 337, 556, doi: [10.1126/science.1223269](https://doi.org/10.1126/science.1223269)
- Casagrande, L., & Vandenberg, D. A. 2018, *MNRAS*, 479, L102, doi: [10.1093/mnrasl/sly104](https://doi.org/10.1093/mnrasl/sly104)
- Chakraborty, A., Roy, A., Sharma, R., et al. 2018, *AJ*, 156, 3, doi: [10.3847/1538-3881/aac436](https://doi.org/10.3847/1538-3881/aac436)
- Chaplin, W. J., Sanchis-Ojeda, R., Campante, T. L., et al. 2013, *ApJ*, 766, 101, doi: [10.1088/0004-637X/766/2/101](https://doi.org/10.1088/0004-637X/766/2/101)
- Chen, J., & Kipping, D. 2017, *ApJ*, 834, 17, doi: [10.3847/1538-4357/834/1/17](https://doi.org/10.3847/1538-4357/834/1/17)
- Christiansen, J. L., Vanderburg, A., Burt, J., et al. 2017, *AJ*, 154, 122, doi: [10.3847/1538-3881/aa832d](https://doi.org/10.3847/1538-3881/aa832d)
- Christiansen, J. L., Crossfield, I. J. M., Barentsen, G., et al. 2018, *AJ*, 155, 57, doi: [10.3847/1538-3881/aa9be0](https://doi.org/10.3847/1538-3881/aa9be0)
- Cieza, L., Padgett, D. L., Stapelfeldt, K. R., et al. 2007, *ApJ*, 667, 308, doi: [10.1086/520698](https://doi.org/10.1086/520698)
- Cochran, W. D., Fabrycky, D. C., Torres, G., et al. 2011, *ApJS*, 197, 7, doi: [10.1088/0067-0049/197/1/7](https://doi.org/10.1088/0067-0049/197/1/7)
- Crossfield, I. J. M., Ciardi, D. R., Petigura, E. A., et al. 2016, *ApJS*, 226, 7, doi: [10.3847/0067-0049/226/1/7](https://doi.org/10.3847/0067-0049/226/1/7)
- Crossfield, I. J. M., Ciardi, D. R., Isaacson, H., et al. 2017, *AJ*, 153, 255, doi: [10.3847/1538-3881/aa6e01](https://doi.org/10.3847/1538-3881/aa6e01)
- Dai, F., Masuda, K., Winn, J. N., & Zeng, L. 2019, *ApJ*, 883, 79, doi: [10.3847/1538-4357/ab3a3b](https://doi.org/10.3847/1538-4357/ab3a3b)
- Dai, F., Winn, J. N., Albrecht, S., et al. 2016, *ApJ*, 823, 115, doi: [10.3847/0004-637X/823/2/115](https://doi.org/10.3847/0004-637X/823/2/115)
- Dai, F., Winn, J. N., Gandolfi, D., et al. 2017, *AJ*, 154, 226, doi: [10.3847/1538-3881/aa9065](https://doi.org/10.3847/1538-3881/aa9065)
- Dai, F., Howard, A. W., Batalha, N. M., et al. 2021, arXiv e-prints, arXiv:2105.08844, <https://arxiv.org/abs/2105.08844>
- Damasso, M., Zeng, L., Malavolta, L., et al. 2019, *A&A*, 624, A38, doi: [10.1051/0004-6361/201834671](https://doi.org/10.1051/0004-6361/201834671)
- David, T. J., Contardo, G., Sandoval, A., et al. 2021, *AJ*, 161, 265, doi: [10.3847/1538-3881/abf439](https://doi.org/10.3847/1538-3881/abf439)
- Díaz, M. R., Jenkins, J. S., Gandolfi, D., et al. 2020, *MNRAS*, 493, 973, doi: [10.1093/mnras/staa277](https://doi.org/10.1093/mnras/staa277)
- Dragomir, D., Teske, J., Günther, M. N., et al. 2019, *ApJL*, 875, L7, doi: [10.3847/2041-8213/ab12ed](https://doi.org/10.3847/2041-8213/ab12ed)
- Dressing, C. D., & Charbonneau, D. 2013, *ApJ*, 767, 95, doi: [10.1088/0004-637X/767/1/95](https://doi.org/10.1088/0004-637X/767/1/95)
- . 2015, *ApJ*, 807, 45, doi: [10.1088/0004-637X/807/1/45](https://doi.org/10.1088/0004-637X/807/1/45)
- Emsenhuber, A., Mordasini, C., Burn, R., et al. 2020a, arXiv e-prints, arXiv:2007.05561, <https://arxiv.org/abs/2007.05561>



- . 2020b, arXiv e-prints, arXiv:2007.05562.  
<https://arxiv.org/abs/2007.05562>
- Espinoza, N., Brahm, R., Jordán, A., et al. 2016, *ApJ*, 830, 43, doi: [10.3847/0004-637X/830/1/43](https://doi.org/10.3847/0004-637X/830/1/43)
- Espinoza, N., Brahm, R., Henning, T., et al. 2020, *MNRAS*, 491, 2982, doi: [10.1093/mnras/stz3150](https://doi.org/10.1093/mnras/stz3150)
- Esposito, M., Armstrong, D. J., Gandolfi, D., et al. 2019, *A&A*, 623, A165, doi: [10.1051/0004-6361/201834853](https://doi.org/10.1051/0004-6361/201834853)
- Esteves, L. J., De Mooij, E. J. W., & Jayawardhana, R. 2015, *ApJ*, 804, 150, doi: [10.1088/0004-637X/804/2/150](https://doi.org/10.1088/0004-637X/804/2/150)
- Evans, D. W., Riello, M., De Angeli, F., et al. 2018, *A&A*, 616, A4, doi: [10.1051/0004-6361/201832756](https://doi.org/10.1051/0004-6361/201832756)
- Fabrycky, D. C., Ford, E. B., Steffen, J. H., et al. 2012, *ApJ*, 750, 114, doi: [10.1088/0004-637X/750/2/114](https://doi.org/10.1088/0004-637X/750/2/114)
- Fedele, D., van den Ancker, M. E., Henning, T., Jayawardhana, R., & Oliveira, J. M. 2010, *A&A*, 510, A72, doi: [10.1051/0004-6361/200912810](https://doi.org/10.1051/0004-6361/200912810)
- Fressin, F., Torres, G., Désert, J.-M., et al. 2011, *ApJS*, 197, 5, doi: [10.1088/0067-0049/197/1/5](https://doi.org/10.1088/0067-0049/197/1/5)
- Fressin, F., Torres, G., Charbonneau, D., et al. 2013, *ApJ*, 766, 81, doi: [10.1088/0004-637X/766/2/81](https://doi.org/10.1088/0004-637X/766/2/81)
- Freudenthal, J., von Essen, C., Ofir, A., et al. 2019, *A&A*, 628, A108, doi: [10.1051/0004-6361/201935879](https://doi.org/10.1051/0004-6361/201935879)
- Fridlund, M., Gaidos, E., Barragán, O., et al. 2017, *A&A*, 604, A16, doi: [10.1051/0004-6361/201730822](https://doi.org/10.1051/0004-6361/201730822)
- Fridlund, M., Livingston, J., Gandolfi, D., et al. 2020, *MNRAS*, 498, 4503, doi: [10.1093/mnras/staa2502](https://doi.org/10.1093/mnras/staa2502)
- Frustagli, G., Poretti, E., Milbourne, T., et al. 2020, *A&A*, 633, A133, doi: [10.1051/0004-6361/201936689](https://doi.org/10.1051/0004-6361/201936689)
- Fulton, B. J., Petigura, E. A., Howard, A. W., et al. 2017, *AJ*, 154, 109, doi: [10.3847/1538-3881/aa80eb](https://doi.org/10.3847/1538-3881/aa80eb)
- Gaia Collaboration, Prusti, T., de Bruijne, J. H. J., et al. 2016, *A&A*, 595, A1, doi: [10.1051/0004-6361/201629272](https://doi.org/10.1051/0004-6361/201629272)
- Gaia Collaboration, Brown, A. G. A., Vallenari, A., et al. 2018, *A&A*, 616, A1, doi: [10.1051/0004-6361/201833051](https://doi.org/10.1051/0004-6361/201833051)
- Gandolfi, D., Barragán, O., Livingston, J. H., et al. 2018, *A&A*, 619, L10, doi: [10.1051/0004-6361/201834289](https://doi.org/10.1051/0004-6361/201834289)
- Gandolfi, D., Fossati, L., Livingston, J. H., et al. 2019, *ApJL*, 876, L24, doi: [10.3847/2041-8213/ab17d9](https://doi.org/10.3847/2041-8213/ab17d9)
- Gautier, Thomas N., I., Charbonneau, D., Rowe, J. F., et al. 2012, *ApJ*, 749, 15, doi: [10.1088/0004-637X/749/1/15](https://doi.org/10.1088/0004-637X/749/1/15)
- Gettel, S., Charbonneau, D., Dressing, C. D., et al. 2016, *ApJ*, 816, 95, doi: [10.3847/0004-637X/816/2/95](https://doi.org/10.3847/0004-637X/816/2/95)
- Gilliland, R. L., Marcy, G. W., Rowe, J. F., et al. 2013, *ApJ*, 766, 40, doi: [10.1088/0004-637X/766/1/40](https://doi.org/10.1088/0004-637X/766/1/40)
- Gillon, M., Demory, B.-O., Van Grootel, V., et al. 2017, *Nature Astronomy*, 1, 0056, doi: [10.1038/s41550-017-0056](https://doi.org/10.1038/s41550-017-0056)
- Ginzburg, S., Schlichting, H. E., & Sari, R. 2016, *ApJ*, 825, 29, doi: [10.3847/0004-637X/825/1/29](https://doi.org/10.3847/0004-637X/825/1/29)
- . 2018, *MNRAS*, 476, 759, doi: [10.1093/mnras/sty290](https://doi.org/10.1093/mnras/sty290)
- Guenther, E. W., Barragán, O., Dai, F., et al. 2017, *A&A*, 608, A93, doi: [10.1051/0004-6361/201730885](https://doi.org/10.1051/0004-6361/201730885)
- Hadden, S., & Lithwick, Y. 2014, *ApJ*, 787, 80, doi: [10.1088/0004-637X/787/1/80](https://doi.org/10.1088/0004-637X/787/1/80)
- . 2017, *AJ*, 154, 5, doi: [10.3847/1538-3881/aa71ef](https://doi.org/10.3847/1538-3881/aa71ef)
- Haisch, Karl E., J., Lada, E. A., & Lada, C. J. 2001, *ApJL*, 553, L153, doi: [10.1086/320685](https://doi.org/10.1086/320685)
- Hambly, N. C., Cropper, M., Boudreault, S., et al. 2018, *A&A*, 616, A15, doi: [10.1051/0004-6361/201832716](https://doi.org/10.1051/0004-6361/201832716)
- Hara, N. C., Bouchy, F., Stalport, M., et al. 2020, *A&A*, 636, L6, doi: [10.1051/0004-6361/201937254](https://doi.org/10.1051/0004-6361/201937254)
- Hartman, J. D., Bakos, G. Á., Kipping, D. M., et al. 2011, *ApJ*, 728, 138, doi: [10.1088/0004-637X/728/2/138](https://doi.org/10.1088/0004-637X/728/2/138)
- Haywood, R. D., Vanderburg, A., Mortier, A., et al. 2018, *AJ*, 155, 203, doi: [10.3847/1538-3881/aab8f3](https://doi.org/10.3847/1538-3881/aab8f3)
- Helled, R., & Fortney, J. J. 2020, *Philosophical Transactions of the Royal Society of London Series A*, 378, 00474, doi: [10.1098/rsta.2019.0474](https://doi.org/10.1098/rsta.2019.0474)
- Hidalgo, D., Pallé, E., Alonso, R., et al. 2020, *A&A*, 636, A89, doi: [10.1051/0004-6361/201937080](https://doi.org/10.1051/0004-6361/201937080)
- Howard, A. W., Johnson, J. A., Marcy, G. W., et al. 2011, *ApJ*, 730, 10, doi: [10.1088/0004-637X/730/1/10](https://doi.org/10.1088/0004-637X/730/1/10)
- Howell, S. B., Rowe, J. F., Bryson, S. T., et al. 2012, *ApJ*, 746, 123, doi: [10.1088/0004-637X/746/2/123](https://doi.org/10.1088/0004-637X/746/2/123)
- Hoyer, S., Gandolfi, D., Armstrong, D. J., et al. 2021, arXiv e-prints, arXiv:2105.01944.  
<https://arxiv.org/abs/2105.01944>
- Hsu, D. C., Ford, E. B., Ragozzine, D., & Ashby, K. 2019, *AJ*, 158, 109, doi: [10.3847/1538-3881/ab31ab](https://doi.org/10.3847/1538-3881/ab31ab)
- Hsu, D. C., Ford, E. B., & Terrien, R. 2020, *MNRAS*, 498, 2249, doi: [10.1093/mnras/staa2391](https://doi.org/10.1093/mnras/staa2391)
- Huang, C. X., Burt, J., Vanderburg, A., et al. 2018, *ApJL*, 868, L39, doi: [10.3847/2041-8213/aaef91](https://doi.org/10.3847/2041-8213/aaef91)
- Hubickyj, O., Bodenheimer, P., & Lissauer, J. J. 2005, *Icarus*, 179, 415, doi: [10.1016/j.icarus.2005.06.021](https://doi.org/10.1016/j.icarus.2005.06.021)
- Ida, S., & Lin, D. N. C. 2005, *ApJ*, 626, 1045, doi: [10.1086/429953](https://doi.org/10.1086/429953)
- Ikoma, M., & Hori, Y. 2012, *ApJ*, 753, 66, doi: [10.1088/0004-637X/753/1/66](https://doi.org/10.1088/0004-637X/753/1/66)
- Izidoro, A., Ogihara, M., Raymond, S. N., et al. 2017, *MNRAS*, 470, 1750, doi: [10.1093/mnras/stx1232](https://doi.org/10.1093/mnras/stx1232)
- Johnson, J. A., Petigura, E. A., Fulton, B. J., et al. 2017, *AJ*, 154, 108, doi: [10.3847/1538-3881/aa80e7](https://doi.org/10.3847/1538-3881/aa80e7)
- Jordán, A., Bakos, G. Á., Bayliss, D., et al. 2020, *AJ*, 160, 222, doi: [10.3847/1538-3881/aba530](https://doi.org/10.3847/1538-3881/aba530)
- Kane, S. R., Yalçınkaya, S., Osborn, H. P., et al. 2020, *AJ*, 160, 129, doi: [10.3847/1538-3881/aba835](https://doi.org/10.3847/1538-3881/aba835)

- Kanodia, S., Wolfgang, A., Stefansson, G. K., Ning, B., & Mahadevan, S. 2019, *ApJ*, 882, 38, doi: [10.3847/1538-4357/ab334c](https://doi.org/10.3847/1538-4357/ab334c)
- King, G. W., & Wheatley, P. J. 2021, *MNRAS*, 501, L28, doi: [10.1093/mnras/slaa186](https://doi.org/10.1093/mnras/slaa186)
- Kipping, D., Nesvorný, D., Hartman, J., et al. 2019, *MNRAS*, 486, 4980, doi: [10.1093/mnras/stz1141](https://doi.org/10.1093/mnras/stz1141)
- Kleine, T., Touboul, M., Bourdon, B., et al. 2009, *GeoCoA*, 73, 5150, doi: [10.1016/j.gca.2008.11.047](https://doi.org/10.1016/j.gca.2008.11.047)
- Kokubo, E., & Ida, S. 2000, *Icarus*, 143, 15, doi: [10.1006/icar.1999.6237](https://doi.org/10.1006/icar.1999.6237)
- Kosiarek, M. R., Blunt, S., López-Morales, M., et al. 2019, *AJ*, 157, 116, doi: [10.3847/1538-3881/aafe83](https://doi.org/10.3847/1538-3881/aafe83)
- Lacedelli, G., Malavolta, L., Borsato, L., et al. 2021, *MNRAS*, 501, 4148, doi: [10.1093/mnras/staa3728](https://doi.org/10.1093/mnras/staa3728)
- Lallement, R., Capitanio, L., Ruiz-Dern, L., et al. 2018, *A&A*, 616, A132, doi: [10.1051/0004-6361/201832832](https://doi.org/10.1051/0004-6361/201832832)
- Lam, K. W. F., Santerne, A., Sousa, S. G., et al. 2018, *A&A*, 620, A77, doi: [10.1051/0004-6361/201834073](https://doi.org/10.1051/0004-6361/201834073)
- Lammer, H., Brasser, R., Johansen, A., Scherf, M., & Leitzinger, M. 2021, *SSRv*, 217, 7, doi: [10.1007/s11214-020-00778-4](https://doi.org/10.1007/s11214-020-00778-4)
- Laughlin, G., Bodenheimer, P., & Adams, F. C. 2004, *ApJL*, 612, L73, doi: [10.1086/424384](https://doi.org/10.1086/424384)
- Lee, E. J., & Chiang, E. 2015, *ApJ*, 811, 41, doi: [10.1088/0004-637X/811/1/41](https://doi.org/10.1088/0004-637X/811/1/41)
- Lee, E. J., & Connors, N. J. 2021, *ApJ*, 908, 32, doi: [10.3847/1538-4357/abd6c7](https://doi.org/10.3847/1538-4357/abd6c7)
- Léger, A., Rouan, D., Schneider, J., et al. 2009, *A&A*, 506, 287, doi: [10.1051/0004-6361/200911933](https://doi.org/10.1051/0004-6361/200911933)
- Lissauer, J. J., Ragozzine, D., Fabrycky, D. C., et al. 2011a, *ApJS*, 197, 8, doi: [10.1088/0067-0049/197/1/8](https://doi.org/10.1088/0067-0049/197/1/8)
- Lissauer, J. J., Fabrycky, D. C., Ford, E. B., et al. 2011b, *Nature*, 470, 53, doi: [10.1038/nature09760](https://doi.org/10.1038/nature09760)
- Lissauer, J. J., Marcy, G. W., Rowe, J. F., et al. 2012, *ApJ*, 750, 112, doi: [10.1088/0004-637X/750/2/112](https://doi.org/10.1088/0004-637X/750/2/112)
- Lithwick, Y., Xie, J., & Wu, Y. 2012, *ApJ*, 761, 122, doi: [10.1088/0004-637X/761/2/122](https://doi.org/10.1088/0004-637X/761/2/122)
- Lopez, E. D., & Fortney, J. J. 2013, *ApJ*, 776, 2, doi: [10.1088/0004-637X/776/1/2](https://doi.org/10.1088/0004-637X/776/1/2)
- . 2014, *ApJ*, 792, 1, doi: [10.1088/0004-637X/792/1/1](https://doi.org/10.1088/0004-637X/792/1/1)
- Lopez, E. D., Fortney, J. J., & Miller, N. 2012, *ApJ*, 761, 59, doi: [10.1088/0004-637X/761/1/59](https://doi.org/10.1088/0004-637X/761/1/59)
- Lopez, T. A., Barros, S. C. C., Santerne, A., et al. 2019, *A&A*, 631, A90, doi: [10.1051/0004-6361/201936267](https://doi.org/10.1051/0004-6361/201936267)
- López-Morales, M., Haywood, R. D., Coughlin, J. L., et al. 2016, *AJ*, 152, 204, doi: [10.3847/0004-6256/152/6/204](https://doi.org/10.3847/0004-6256/152/6/204)
- Luque, R., Nowak, G., Pallé, E., et al. 2019, *A&A*, 623, A114, doi: [10.1051/0004-6361/201834952](https://doi.org/10.1051/0004-6361/201834952)
- Luri, X., Brown, A. G. A., Sarro, L. M., et al. 2018, *A&A*, 616, A9, doi: [10.1051/0004-6361/201832964](https://doi.org/10.1051/0004-6361/201832964)
- Malavolta, L., Borsato, L., Granata, V., et al. 2017, *AJ*, 153, 224, doi: [10.3847/1538-3881/aa6897](https://doi.org/10.3847/1538-3881/aa6897)
- Malavolta, L., Mayo, A. W., Louden, T., et al. 2018, *AJ*, 155, 107, doi: [10.3847/1538-3881/aaa5b5](https://doi.org/10.3847/1538-3881/aaa5b5)
- Marcy, G. W., Isaacson, H., Howard, A. W., et al. 2014, *ApJS*, 210, 20, doi: [10.1088/0067-0049/210/2/20](https://doi.org/10.1088/0067-0049/210/2/20)
- Marrese, P. M., Marinoni, S., Fabrizio, M., & Altavilla, G. 2019, *A&A*, 621, A144, doi: [10.1051/0004-6361/201834142](https://doi.org/10.1051/0004-6361/201834142)
- Masuda, K. 2014, *ApJ*, 783, 53, doi: [10.1088/0004-637X/783/1/53](https://doi.org/10.1088/0004-637X/783/1/53)
- Mayo, A. W., Vanderburg, A., Latham, D. W., et al. 2018, *AJ*, 155, 136, doi: [10.3847/1538-3881/aaadff](https://doi.org/10.3847/1538-3881/aaadff)
- Mayo, A. W., Rajpaul, V. M., Buchhave, L. A., et al. 2019, *AJ*, 158, 165, doi: [10.3847/1538-3881/ab3e2f](https://doi.org/10.3847/1538-3881/ab3e2f)
- McArthur, B. E., Endl, M., Cochran, W. D., et al. 2004, *ApJL*, 614, L81, doi: [10.1086/425561](https://doi.org/10.1086/425561)
- Mills, S. M., & Mazeh, T. 2017, *ApJL*, 839, L8, doi: [10.3847/2041-8213/aa67eb](https://doi.org/10.3847/2041-8213/aa67eb)
- Mills, S. M., Howard, A. W., Weiss, L. M., et al. 2019, *AJ*, 157, 145, doi: [10.3847/1538-3881/ab0899](https://doi.org/10.3847/1538-3881/ab0899)
- Montet, B. T., Morton, T. D., Foreman-Mackey, D., et al. 2015, *ApJ*, 809, 25, doi: [10.1088/0004-637X/809/1/25](https://doi.org/10.1088/0004-637X/809/1/25)
- Mortier, A., Bonomo, A. S., Rajpaul, V. M., et al. 2018, *MNRAS*, 481, 1839, doi: [10.1093/mnras/sty2360](https://doi.org/10.1093/mnras/sty2360)
- Mortier, A., Zapatero Osorio, M. R., Malavolta, L., et al. 2020, *MNRAS*, 499, 5004, doi: [10.1093/mnras/staa3144](https://doi.org/10.1093/mnras/staa3144)
- Morton, T. D., Bryson, S. T., Coughlin, J. L., et al. 2016, *ApJ*, 822, 86, doi: [10.3847/0004-637X/822/2/86](https://doi.org/10.3847/0004-637X/822/2/86)
- Motalebi, F., Udry, S., Gillon, M., et al. 2015, *A&A*, 584, A72, doi: [10.1051/0004-6361/201526822](https://doi.org/10.1051/0004-6361/201526822)
- Moutou, C., Almenara, J. M., Díaz, R. F., et al. 2014, *MNRAS*, 444, 2783, doi: [10.1093/mnras/stu1645](https://doi.org/10.1093/mnras/stu1645)
- Murray-Clay, R. A., Chiang, E. I., & Murray, N. 2009, *ApJ*, 693, 23, doi: [10.1088/0004-637X/693/1/23](https://doi.org/10.1088/0004-637X/693/1/23)
- Narita, N., Hirano, T., Fukui, A., et al. 2017, *PASJ*, 69, 29, doi: [10.1093/pasj/psx002](https://doi.org/10.1093/pasj/psx002)
- Neil, A. R., & Rogers, L. A. 2020, *ApJ*, 891, 12, doi: [10.3847/1538-4357/ab6a92](https://doi.org/10.3847/1538-4357/ab6a92)
- Nesvorný, D., Kipping, D. M., Buchhave, L. A., et al. 2012, *Science*, 336, 1133, doi: [10.1126/science.1221141](https://doi.org/10.1126/science.1221141)
- Nielsen, L. D., Gandolfi, D., Armstrong, D. J., et al. 2020, *MNRAS*, 492, 5399, doi: [10.1093/mnras/staa197](https://doi.org/10.1093/mnras/staa197)
- Ning, B., Wolfgang, A., & Ghosh, S. 2018, *ApJ*, 869, 5, doi: [10.3847/1538-4357/aaeb31](https://doi.org/10.3847/1538-4357/aaeb31)
- Ochsenbein, F., Bauer, P., & Marcout, J. 2000, *A&AS*, 143, 23, doi: [10.1051/aas:2000169](https://doi.org/10.1051/aas:2000169)

- Ofir, A., Dreizler, S., Zechmeister, M., & Husser, T.-O. 2014, *A&A*, 561, A103, doi: [10.1051/0004-6361/201220935](https://doi.org/10.1051/0004-6361/201220935)
- Ogihara, M., Kunitomo, M., & Hori, Y. 2020, *ApJ*, 899, 91, doi: [10.3847/1538-4357/aba75e](https://doi.org/10.3847/1538-4357/aba75e)
- Ormel, C. W., Vazan, A., & Brouwers, M. G. 2021, *A&A*, 647, A175, doi: [10.1051/0004-6361/202039706](https://doi.org/10.1051/0004-6361/202039706)
- Osborn, H. P., Santerne, A., Barros, S. C. C., et al. 2017, *A&A*, 604, A19, doi: [10.1051/0004-6361/201628932](https://doi.org/10.1051/0004-6361/201628932)
- Osborn, H. P., Armstrong, D. J., Adibekyan, V., et al. 2021, *MNRAS*, 502, 4842, doi: [10.1093/mnras/stab182](https://doi.org/10.1093/mnras/stab182)
- Otegi, J. F., Bouchy, F., & Helled, R. 2020, *A&A*, 634, A43, doi: [10.1051/0004-6361/201936482](https://doi.org/10.1051/0004-6361/201936482)
- Owen, J. E., & Jackson, A. P. 2012, *MNRAS*, 425, 2931, doi: [10.1111/j.1365-2966.2012.21481.x](https://doi.org/10.1111/j.1365-2966.2012.21481.x)
- Owen, J. E., & Wu, Y. 2013, *ApJ*, 775, 105, doi: [10.1088/0004-637X/775/2/105](https://doi.org/10.1088/0004-637X/775/2/105)
- . 2016, *ApJ*, 817, 107, doi: [10.3847/0004-637X/817/2/107](https://doi.org/10.3847/0004-637X/817/2/107)
- . 2017, *ApJ*, 847, 29, doi: [10.3847/1538-4357/aa890a](https://doi.org/10.3847/1538-4357/aa890a)
- Palatnick, S., Kipping, D., & Yahalomi, D. 2021, *ApJL*, 909, L6, doi: [10.3847/2041-8213/abe0bb](https://doi.org/10.3847/2041-8213/abe0bb)
- Palle, E., Nowak, G., Luque, R., et al. 2019, *A&A*, 623, A41, doi: [10.1051/0004-6361/201834001](https://doi.org/10.1051/0004-6361/201834001)
- Panichi, F., Migaszewski, C., & Goździewski, K. 2019, *MNRAS*, 485, 4601, doi: [10.1093/mnras/stz721](https://doi.org/10.1093/mnras/stz721)
- Pecaut, M. J., & Mamajek, E. E. 2013, *ApJS*, 208, 9, doi: [10.1088/0067-0049/208/1/9](https://doi.org/10.1088/0067-0049/208/1/9)
- Pepper, J., Gould, A., & Depoy, D. L. 2003, *AcA*, 53, 213. <https://arxiv.org/abs/astro-ph/0208042>
- Persson, C. M., Fridlund, M., Barragán, O., et al. 2018, *A&A*, 618, A33, doi: [10.1051/0004-6361/201832867](https://doi.org/10.1051/0004-6361/201832867)
- Petigura, E. A., Howard, A. W., Lopez, E. D., et al. 2016, *ApJ*, 818, 36, doi: [10.3847/0004-637X/818/1/36](https://doi.org/10.3847/0004-637X/818/1/36)
- Petigura, E. A., Sinukoff, E., Lopez, E. D., et al. 2017, *AJ*, 153, 142, doi: [10.3847/1538-3881/aa5ea5](https://doi.org/10.3847/1538-3881/aa5ea5)
- Petigura, E. A., Benneke, B., Batygin, K., et al. 2018, *AJ*, 156, 89, doi: [10.3847/1538-3881/aaceac](https://doi.org/10.3847/1538-3881/aaceac)
- Podolak, M., Helled, R., & Schubert, G. 2019, *MNRAS*, 487, 2653, doi: [10.1093/mnras/stz1467](https://doi.org/10.1093/mnras/stz1467)
- Pollack, J. B., Hubickyj, O., Bodenheimer, P., et al. 1996, *Icarus*, 124, 62, doi: [10.1006/icar.1996.0190](https://doi.org/10.1006/icar.1996.0190)
- Quinn, S. N., Becker, J. C., Rodriguez, J. E., et al. 2019, *AJ*, 158, 177, doi: [10.3847/1538-3881/ab3f2b](https://doi.org/10.3847/1538-3881/ab3f2b)
- R Core Team. 2020, *R: A Language and Environment for Statistical Computing*, R Foundation for Statistical Computing, Vienna, Austria. <https://www.R-project.org/>
- Rajpaul, V., Buchhave, L. A., & Aigrain, S. 2017, *MNRAS*, 471, L125, doi: [10.1093/mnrasl/slx116](https://doi.org/10.1093/mnrasl/slx116)
- Riello, M., De Angeli, F., Evans, D. W., et al. 2018, *A&A*, 616, A3, doi: [10.1051/0004-6361/201832712](https://doi.org/10.1051/0004-6361/201832712)
- Rogers, J. G., & Owen, J. E. 2021, *MNRAS*, 503, 1526, doi: [10.1093/mnras/stab529](https://doi.org/10.1093/mnras/stab529)
- Rowe, J. F., Bryson, S. T., Marcy, G. W., et al. 2014, *ApJ*, 784, 45, doi: [10.1088/0004-637X/784/1/45](https://doi.org/10.1088/0004-637X/784/1/45)
- Saad-Olivera, X., Nesvorný, D., Kipping, D. M., & Roig, F. 2017, *AJ*, 153, 198, doi: [10.3847/1538-3881/aa64e0](https://doi.org/10.3847/1538-3881/aa64e0)
- Sanchis-Ojeda, R., Rappaport, S., Winn, J. N., et al. 2013, *ApJ*, 774, 54, doi: [10.1088/0004-637X/774/1/54](https://doi.org/10.1088/0004-637X/774/1/54)
- Sanchis-Ojeda, R., Fabrycky, D. C., Winn, J. N., et al. 2012, *Nature*, 487, 449, doi: [10.1038/nature11301](https://doi.org/10.1038/nature11301)
- Schlecker, M., Pham, D., Burn, R., et al. 2021, arXiv e-prints, arXiv:2104.11750. <https://arxiv.org/abs/2104.11750>
- Schmitt, J. R., Agol, E., Deck, K. M., et al. 2014, *ApJ*, 795, 167, doi: [10.1088/0004-637X/795/2/167](https://doi.org/10.1088/0004-637X/795/2/167)
- Sinukoff, E., Howard, A. W., Petigura, E. A., et al. 2016, *ApJ*, 827, 78, doi: [10.3847/0004-637X/827/1/78](https://doi.org/10.3847/0004-637X/827/1/78)
- . 2017, *AJ*, 153, 271, doi: [10.3847/1538-3881/aa725f](https://doi.org/10.3847/1538-3881/aa725f)
- Smith, A. M. S., Acton, J. S., Anderson, D. R., et al. 2021, *A&A*, 646, A183, doi: [10.1051/0004-6361/202039712](https://doi.org/10.1051/0004-6361/202039712)
- Sozzetti, A., Damasso, M., Bonomo, A. S., et al. 2021, *A&A*, 648, A75, doi: [10.1051/0004-6361/202040034](https://doi.org/10.1051/0004-6361/202040034)
- Steffen, J. H. 2016, *MNRAS*, 457, 4384, doi: [10.1093/mnras/stw241](https://doi.org/10.1093/mnras/stw241)
- Steffen, J. H., Fabrycky, D. C., Ford, E. B., et al. 2012, *MNRAS*, 421, 2342, doi: [10.1111/j.1365-2966.2012.20467.x](https://doi.org/10.1111/j.1365-2966.2012.20467.x)
- Steffen, J. H., Fabrycky, D. C., Agol, E., et al. 2013, *MNRAS*, 428, 1077, doi: [10.1093/mnras/sts090](https://doi.org/10.1093/mnras/sts090)
- Sun, L., Ioannidis, P., Gu, S., et al. 2019, *A&A*, 624, A15, doi: [10.1051/0004-6361/201834275](https://doi.org/10.1051/0004-6361/201834275)
- Taylor, M. B. 2005, in *Astronomical Society of the Pacific Conference Series*, Vol. 347, *Astronomical Data Analysis Software and Systems XIV*, ed. P. Shopbell, M. Britton, & R. Ebert, 29
- Teske, J., Xuesong Wang, S., Wolfgang, A., et al. 2020a, arXiv e-prints, arXiv:2011.11560. <https://arxiv.org/abs/2011.11560>
- Teske, J., Díaz, M. R., Luque, R., et al. 2020b, *AJ*, 160, 96, doi: [10.3847/1538-3881/ab9f95](https://doi.org/10.3847/1538-3881/ab9f95)
- Thompson, S. E., Coughlin, J. L., Hoffman, K., et al. 2018, *ApJS*, 235, 38, doi: [10.3847/1538-4365/aab4f9](https://doi.org/10.3847/1538-4365/aab4f9)
- Trifonov, T., Rybizki, J., & Kürster, M. 2019, *A&A*, 622, L7, doi: [10.1051/0004-6361/201834817](https://doi.org/10.1051/0004-6361/201834817)
- Udry, S., Dumusque, X., Lovis, C., et al. 2019, *A&A*, 622, A37, doi: [10.1051/0004-6361/201731173](https://doi.org/10.1051/0004-6361/201731173)

- Ulmer-Moll, S., Santos, N. C., Figueira, P., Brinchmann, J., & Faria, J. P. 2019, *A&A*, 630, A135, doi: [10.1051/0004-6361/201936049](https://doi.org/10.1051/0004-6361/201936049)
- Van Eylen, V., & Albrecht, S. 2015, *ApJ*, 808, 126, doi: [10.1088/0004-637X/808/2/126](https://doi.org/10.1088/0004-637X/808/2/126)
- Van Eylen, V., Nowak, G., Albrecht, S., et al. 2016, *ApJ*, 820, 56, doi: [10.3847/0004-637X/820/1/56](https://doi.org/10.3847/0004-637X/820/1/56)
- Van Eylen, V., Dai, F., Mathur, S., et al. 2018, *MNRAS*, 478, 4866, doi: [10.1093/mnras/sty1390](https://doi.org/10.1093/mnras/sty1390)
- Van Grootel, V., Gillon, M., Valencia, D., et al. 2014, *ApJ*, 786, 2, doi: [10.1088/0004-637X/786/1/2](https://doi.org/10.1088/0004-637X/786/1/2)
- Vanderburg, A., Montet, B. T., Johnson, J. A., et al. 2015, *ApJ*, 800, 59, doi: [10.1088/0004-637X/800/1/59](https://doi.org/10.1088/0004-637X/800/1/59)
- Vanderburg, A., Bieryla, A., Duvvuri, D. A., et al. 2016, *ApJL*, 829, L9, doi: [10.3847/2041-8205/829/1/L9](https://doi.org/10.3847/2041-8205/829/1/L9)
- Vanderburg, A., Becker, J. C., Buchhave, L. A., et al. 2017, *AJ*, 154, 237, doi: [10.3847/1538-3881/aa918b](https://doi.org/10.3847/1538-3881/aa918b)
- Venturini, J., Guilera, O. M., Haldemann, J., Ronco, M. P., & Mordasini, C. 2020a, *A&A*, 643, L1, doi: [10.1051/0004-6361/202039141](https://doi.org/10.1051/0004-6361/202039141)
- Venturini, J., Guilera, O. M., Ronco, M. P., & Mordasini, C. 2020b, *A&A*, 644, A174, doi: [10.1051/0004-6361/202039140](https://doi.org/10.1051/0004-6361/202039140)
- Vissapragada, S., Jontof-Hutter, D., Shporer, A., et al. 2020, *AJ*, 159, 108, doi: [10.3847/1538-3881/ab65c8](https://doi.org/10.3847/1538-3881/ab65c8)
- Wang, J., Xie, J.-W., Barclay, T., & Fischer, D. A. 2014, *ApJ*, 783, 4, doi: [10.1088/0004-637X/783/1/4](https://doi.org/10.1088/0004-637X/783/1/4)
- Weiss, L. M., & Marcy, G. W. 2014, *ApJL*, 783, L6, doi: [10.1088/2041-8205/783/1/L6](https://doi.org/10.1088/2041-8205/783/1/L6)
- Weiss, L. M., Marcy, G. W., Rowe, J. F., et al. 2013, *ApJ*, 768, 14, doi: [10.1088/0004-637X/768/1/14](https://doi.org/10.1088/0004-637X/768/1/14)
- Weiss, L. M., Dai, F., Huber, D., et al. 2021, *AJ*, 161, 56, doi: [10.3847/1538-3881/abd409](https://doi.org/10.3847/1538-3881/abd409)
- Wenger, M., Ochsenbein, F., Egret, D., et al. 2000, *A&AS*, 143, 9, doi: [10.1051/aas:2000332](https://doi.org/10.1051/aas:2000332)
- West, R. G., Gillen, E., Bayliss, D., et al. 2019, *MNRAS*, 486, 5094, doi: [10.1093/mnras/stz1084](https://doi.org/10.1093/mnras/stz1084)
- Wolfgang, A., Rogers, L. A., & Ford, E. B. 2016, *ApJ*, 825, 19, doi: [10.3847/0004-637X/825/1/19](https://doi.org/10.3847/0004-637X/825/1/19)
- Wu, Y., & Lithwick, Y. 2013, *ApJ*, 772, 74, doi: [10.1088/0004-637X/772/1/74](https://doi.org/10.1088/0004-637X/772/1/74)
- Xie, J.-W. 2013, *ApJS*, 208, 22, doi: [10.1088/0067-0049/208/2/22](https://doi.org/10.1088/0067-0049/208/2/22)
- . 2014, *ApJS*, 210, 25, doi: [10.1088/0067-0049/210/2/25](https://doi.org/10.1088/0067-0049/210/2/25)
- Yoffe, G., Ofir, A., & Aharonson, O. 2021, *ApJ*, 908, 114, doi: [10.3847/1538-4357/abc87a](https://doi.org/10.3847/1538-4357/abc87a)
- Youdin, A. N. 2011, *ApJ*, 742, 38, doi: [10.1088/0004-637X/742/1/38](https://doi.org/10.1088/0004-637X/742/1/38)
- Yu, L., Rodriguez, J. E., Eastman, J. D., et al. 2018, *AJ*, 156, 127, doi: [10.3847/1538-3881/aad6e7](https://doi.org/10.3847/1538-3881/aad6e7)
- Zeng, L., Jacobsen, S. B., Sasselov, D. D., et al. 2019, *Proceedings of the National Academy of Science*, 116, 9723, doi: [10.1073/pnas.1812905116](https://doi.org/10.1073/pnas.1812905116)

Table 1. Periods, Masses, Radii, and Occurrences for Transiting Exoplanets with  $M_p \lesssim 20 M_\oplus$ 

Host Star	Gaia DR2	Exoplanet	Period	Mass	Radius	Occurrence	Mass	Discovery	Parameter
Simbad Name	Source ID	Name	(days)	( $M_\oplus$ )	( $R_\oplus$ )			Reference	Reference
Kepler-131	2102110174677569664	Kepler-131 b	16.092	$16.1^{+3.5}_{-3.0}$	$2.41^{+0.20}_{-0.20}$	0.036	Doppler	Marcy et al. (2014)	Marcy et al. (2014)
Kepler-131	2102110174677569664	Kepler-131 c	25.5169	$8.2^{+5.9}_{-5.9}$	$0.84^{+0.07}_{-0.07}$	0.094	Doppler	Marcy et al. (2014)	Marcy et al. (2014)
BD+41 3306	2101486923385239808	Kepler-444 d	6.189	$0.2^{+0.5}_{-0.1}$	$0.75^{+0.02}_{-0.02}$	0.061	TTV	Campante et al. (2015)	Hadden & Lithwick (2017)
BD+41 3306	2101486923385239808	Kepler-444 e	7.743	$0.1^{+0.2}_{-0.1}$	$0.73^{+0.02}_{-0.02}$	0.065	TTV	Campante et al. (2015)	Hadden & Lithwick (2017)
Kepler-10	2132155017099178624	Kepler-10 b	0.837491	$4.6^{+1.3}_{-1.5}$	$1.48^{+0.03}_{-0.03}$	0.0013	Doppler	Batalha et al. (2011)	Esteves et al. (2015)
Kepler-10	2132155017099178624	Kepler-10 c	45.2946	$7.4^{+1.3}_{-1.2}$	$2.62^{+0.05}_{-0.03}$	0.06	Doppler	Fressin et al. (2011)	Rajpaul et al. (2017)
Kepler-106	2082074942519913344	Kepler-106 c	13.5708	$10.4^{+3.2}_{-3.2}$	$2.50^{+0.32}_{-0.32}$	0.031	Doppler	Marcy et al. (2014)	Marcy et al. (2014)
Kepler-106	2082074942519913344	Kepler-106 e	43.8445	$11.2^{+5.8}_{-5.8}$	$2.56^{+0.33}_{-0.33}$	0.057	Doppler	Marcy et al. (2014)	Marcy et al. (2014)
Kepler-289	2078515170549178880	Kepler-289 b	34.545	$7.3^{+6.8}_{-6.8}$	$2.15^{+0.10}_{-0.10}$	0.042	TTV	Rowe et al. (2014)	Schmitt et al. (2014)
Kepler-289	2078515170549178880	Kepler-289 d	66.0634	$4.0^{+0.9}_{-0.9}$	$2.68^{+0.17}_{-0.17}$	0.056	TTV	Schmitt et al. (2014)	Schmitt et al. (2014)
K2-263	657756997089784960	K2-263 b	50.818947	$14.8^{+3.1}_{-3.1}$	$2.41^{+0.12}_{-0.12}$	0.055	Doppler	Mortier et al. (2018)	Mortier et al. (2018)
Kepler-538	2087171453788422528	Kepler-538 b	81.73778	$10.6^{+2.5}_{-2.4}$	$2.21^{+0.04}_{-0.04}$	0.055	Doppler	Morton et al. (2016)	Mayo et al. (2019)
Kepler-549	2107622335702262400	Kepler-549 b	42.95	$11.0^{+4.2}_{-3.2}$	$2.87^{+0.08}_{-0.08}$	0.054	TTV	Morton et al. (2016)	Hadden & Lithwick (2016)
Kepler-310	2127798442794047104	Kepler-310 d	92.874	$7.0^{+3.4}_{-3.1}$	$2.44^{+0.06}_{-0.06}$	0.053	TTV	Rowe et al. (2014)	Hadden & Lithwick (2016)
HD 21749	4673947174316727040	GJ 143 b	35.61253	$22.7^{+2.1}_{-1.9}$	$2.61^{+0.12}_{-0.12}$	0.052	Doppler	Trifonov et al. (2019)	Dragomir et al. (2019)
TYC 243-1528-1	3850421005290172416	TOI-561 b	0.446578	$1.6^{+0.4}_{-0.4}$	$1.42^{+0.07}_{-0.07}$	0.0014	Doppler	Lacedelli et al. (2021)	Lacedelli et al. (2021)
TYC 243-1528-1	3850421005290172416	TOI-561 c	10.779	$5.4^{+1.0}_{-1.0}$	$2.88^{+0.10}_{-0.10}$	0.02	Doppler	Lacedelli et al. (2021)	Lacedelli et al. (2021)
TYC 243-1528-1	3850421005290172416	TOI-561 d	25.62	$11.9^{+1.3}_{-1.3}$	$2.53^{+0.13}_{-0.13}$	0.047	Doppler	Lacedelli et al. (2021)	Lacedelli et al. (2021)
TYC 243-1528-1	3850421005290172416	TOI-561 e	77.23	$16.0^{+2.3}_{-2.3}$	$2.67^{+0.11}_{-0.11}$	0.051	Doppler	Lacedelli et al. (2021)	Lacedelli et al. (2021)
TYC 243-1528-1	3850421005290172416	TOI-561 f	16.287	$3.0^{+2.4}_{-1.9}$	$2.32^{+0.16}_{-0.16}$	0.038	Doppler	Weiss et al. (2021)	Weiss et al. (2021)
BD+20 594	58200934326315136	BD+20 594 b	41.6855	$16.3^{+6.0}_{-6.0}$	$2.23^{+0.14}_{-0.14}$	0.049	Doppler	Espinoza et al. (2016)	Espinoza et al. (2016)
Kepler-20	2102548708017562112	Kepler-20 b	3.69611525	$9.7^{+1.4}_{-1.4}$	$1.87^{+0.07}_{-0.07}$	0.0039	Doppler	Gautier et al. (2012)	Buchhave et al. (2016)
Kepler-20	2102548708017562112	Kepler-20 c	10.85409089	$12.8^{+2.2}_{-2.2}$	$3.05^{+0.06}_{-0.06}$	0.017	Doppler	Gautier et al. (2012)	Buchhave et al. (2016)
Kepler-20	2102548708017562112	Kepler-20 d	77.61130017	$10.1^{+4.0}_{-3.7}$	$2.74^{+0.07}_{-0.07}$	0.049	Doppler	Gautier et al. (2012)	Buchhave et al. (2016)
Kepler-359	2077683871034907648	Kepler-359 c	57.693	$2.9^{+1.9}_{-1.9}$	$3.61^{+0.18}_{-0.15}$	0.022	TTV	Rowe et al. (2014)	Hadden & Lithwick (2017)
Kepler-359	2077683871034907648	Kepler-359 d	77.083	$2.7^{+2.5}_{-1.5}$	$2.76^{+0.18}_{-0.17}$	0.049	TTV	Rowe et al. (2014)	Hadden & Lithwick (2017)
nu.02 Lup	5902750168276592256	HD 136352 b	11.57779	$4.6^{+0.4}_{-0.4}$	$1.48^{+0.06}_{-0.06}$	0.027	Doppler	Udry et al. (2019)	Kane et al. (2020)
nu.02 Lup	5902750168276592256	HD 136352 c	27.5909	$11.3^{+0.7}_{-0.7}$	$2.61^{+0.08}_{-0.08}$	0.046	Doppler	Udry et al. (2019)	Kane et al. (2020)
K2-138	2413596935442139520	K2-138 b	2.35309	$3.1^{+1.1}_{-1.1}$	$1.51^{+0.11}_{-0.11}$	0.0048	Doppler	Christiansen et al. (2018)	Lopez et al. (2019)
K2-138	2413596935442139520	K2-138 c	3.56004	$6.3^{+1.1}_{-1.2}$	$2.30^{+0.12}_{-0.09}$	0.0038	Doppler	Christiansen et al. (2018)	Lopez et al. (2019)
K2-138	2413596935442139520	K2-138 d	5.40479	$7.9^{+1.4}_{-1.4}$	$2.39^{+0.10}_{-0.10}$	0.0088	Doppler	Christiansen et al. (2018)	Lopez et al. (2019)
K2-138	2413596935442139520	K2-138 e	8.26146	$13.0^{+2.0}_{-2.0}$	$3.39^{+0.16}_{-0.16}$	0.0064	Doppler	Christiansen et al. (2018)	Lopez et al. (2019)
K2-138	2413596935442139520	K2-138 f	12.75758	$1.6^{+2.1}_{-1.2}$	$2.90^{+0.16}_{-0.11}$	0.023	Doppler	Christiansen et al. (2018)	Lopez et al. (2019)
K2-138	2413596935442139520	K2-138 g	41.96797	$4.3^{+5.3}_{-3.0}$	$3.01^{+0.30}_{-0.25}$	0.046	Doppler	Lopez et al. (2019)	Lopez et al. (2019)
Kepler-595	2135237601028549888	Kepler-595 b	25.3029092	$17.4^{+3.8}_{-3.8}$	$3.71^{+0.01}_{-0.01}$	0.018	TTV	Yoffe et al. (2021)	Yoffe et al. (2021)
Kepler-595	2135237601028549888	Kepler-595 c	12.38602	$3.3^{+1.7}_{-1.7}$	$1.01^{+0.02}_{-0.02}$	0.043	TTV	Yoffe et al. (2021)	Yoffe et al. (2021)
HD 23472	4674216245427964416	HD 23472 b	17.667	$17.9^{+1.4}_{-1.4}$	$1.87^{+1.32}_{-1.32}$	0.0095	Doppler	Trifonov et al. (2019)	Trifonov et al. (2019)
HD 23472	4674216245427964416	HD 23472 c	29.625	$17.2^{+13.8}_{-13.8}$	$2.15^{+0.34}_{-0.34}$	0.042	Doppler	Trifonov et al. (2019)	Trifonov et al. (2019)

Table 1 continued



Table 1 (continued)

Host Star	Gaia DR2	Exoplanet	Period	Mass	Radius	Occurrence	Mass	Discovery	Parameter
Simbad Name	Source ID	Name	(days)	( $M_{\oplus}$ )	( $R_{\oplus}$ )			Reference	Reference
Kepler-11	2076960598545789824	Kepler-11 d	22.687	6.8 $^{+0.7}_{-0.7}$	4.04 $^{+0.42}_{-0.42}$	0.014	TTV	Lissauer et al. (2011b)	Hadden & Lithwick (2015)
Kepler-11	2076960598545789824	Kepler-11 e	31.995	6.7 $^{+1.2}_{-1.2}$	4.81 $^{+0.55}_{-0.50}$	0.0067	TTV	Lissauer et al. (2011b)	Hadden & Lithwick (2015)
Kepler-11	2076960598545789824	Kepler-11 f	46.686	1.7 $^{+0.5}_{-0.4}$	3.15 $^{+0.38}_{-0.33}$	0.041	TTV	Lissauer et al. (2011b)	Hadden & Lithwick (2015)
Kepler-30	2100243616248608896	Kepler-30 b	29.323	8.8 $^{+0.6}_{-0.5}$	2.13 $^{+0.14}_{-0.13}$	0.04	TTV	Sanchis-Ojeda et al. (2012)	Hadden & Lithwick (2015)
HD 15337	5068777809824976256	HD 15337 b	4.75615	7.5 $^{+1.0}_{-1.0}$	1.64 $^{+0.08}_{-0.06}$	0.01	Doppler	Gandolfi et al. (2019)	Gandolfi et al. (2019)
HD 15337	5068777809824976256	HD 15337 c	17.1784	8.1 $^{+1.8}_{-1.7}$	2.39 $^{+0.12}_{-0.12}$	0.039	Doppler	Gandolfi et al. (2019)	Gandolfi et al. (2019)
HD 3167	2554032474712538880	HD 3167 b	0.96	5.6 $^{+1.0}_{-1.0}$	1.63 $^{+0.05}_{-0.05}$	0.00087	Doppler	Vanderburg et al. (2016)	Dai et al. (2019)
HD 3167	2554032474712538880	HD 3167 c	29.8454	9.8 $^{+1.3}_{-1.3}$	3.01 $^{+0.28}_{-0.28}$	0.037	Doppler	Vanderburg et al. (2016)	Christiansen et al. (2015)
Kepler-102	2119583201145735808	Kepler-102 d	10.3117	3.8 $^{+1.8}_{-1.8}$	1.18 $^{+0.04}_{-0.04}$	0.031	Doppler	Marcy et al. (2014)	Marcy et al. (2014)
Kepler-102	2119583201145735808	Kepler-102 e	16.1457	8.9 $^{+2.0}_{-2.0}$	2.22 $^{+0.07}_{-0.07}$	0.037	Doppler	Wang et al. (2014)	Marcy et al. (2014)
BD+48 2893	2129550445852902656	Kepler-68 b	5.3988	7.7 $^{+1.4}_{-1.4}$	2.60 $^{+0.04}_{-0.04}$	0.0089	Doppler	Gilliland et al. (2013)	Mills et al. (2019)
BD+48 2893	2129550445852902656	Kepler-68 c	9.6051	2.0 $^{+1.7}_{-1.7}$	1.04 $^{+0.02}_{-0.02}$	0.035	Doppler	Gilliland et al. (2013)	Mills et al. (2019)
HD 119130	3616931735377523712	K2-292 b	16.9841	24.5 $^{+4.4}_{-4.4}$	2.63 $^{+0.11}_{-0.10}$	0.034	Doppler	Luque et al. (2019)	Luque et al. (2019)
Kepler-79	2076085318570299136	Kepler-79 b	13.484542	12.5 $^{+4.5}_{-3.6}$	3.34 $^{+0.03}_{-0.03}$	0.013	TTV	Yoffe et al. (2021)	Yoffe et al. (2021)
Kepler-79	2076085318570299136	Kepler-79 c	27.4023	9.5 $^{+2.1}_{-2.1}$	3.55 $^{+0.03}_{-0.03}$	0.02	TTV	Yoffe et al. (2021)	Yoffe et al. (2021)
Kepler-79	2076085318570299136	Kepler-79 d	52.090767	11.3 $^{+2.2}_{-2.2}$	6.91 $^{+0.01}_{-0.01}$	0.005	TTV	Yoffe et al. (2021)	Yoffe et al. (2021)
Kepler-79	2076085318570299136	Kepler-79 e	81.064	3.4 $^{+1.0}_{-0.8}$	3.40 $^{+0.12}_{-0.13}$	0.033	TTV	Rowe et al. (2014)	Hadden & Lithwick (2015)
Kepler-48	2075112109039378688	Kepler-48 b	4.778	3.9 $^{+2.1}_{-2.1}$	1.88 $^{+0.10}_{-0.10}$	0.0053	Doppler	Steffen et al. (2013)	Marcy et al. (2014)
Kepler-48	2075112109039378688	Kepler-48 c	9.67395	14.6 $^{+2.3}_{-2.3}$	2.71 $^{+0.14}_{-0.14}$	0.021	Doppler	Steffen et al. (2013)	Marcy et al. (2014)
Kepler-48	2075112109039378688	Kepler-48 d	42.8961	7.9 $^{+4.6}_{-4.6}$	2.04 $^{+0.11}_{-0.11}$	0.031	Doppler	Marcy et al. (2014)	Marcy et al. (2014)
HD 5278	4617759514501503616	HD 5278 b	14.339156	7.8 $^{+1.5}_{-1.5}$	2.45 $^{+0.05}_{-0.05}$	0.033	Doppler	Sozzetti et al. (2021)	Sozzetti et al. (2021)
Kepler-411	2132768952604988672	Kepler-411 b	3.005156	25.6 $^{+2.6}_{-2.6}$	2.40 $^{+0.05}_{-0.05}$	0.002	TTV	Wang et al. (2014)	Sun et al. (2019)
Kepler-411	2132768952604988672	Kepler-411 c	7.834435	26.4 $^{+5.9}_{-5.9}$	4.42 $^{+0.06}_{-0.06}$	0.003	TTV	Morton et al. (2016)	Sun et al. (2019)
Kepler-411	2132768952604988672	Kepler-411 d	58.02035	15.2 $^{+5.1}_{-5.1}$	3.32 $^{+0.10}_{-0.10}$	0.033	TTV	Sun et al. (2019)	Sun et al. (2019)
Kepler-29	2086435189017387264	Kepler-29 b	10.33974	5.0 $^{+1.3}_{-1.3}$	2.55 $^{+0.12}_{-0.12}$	0.023	TTV	Fabrycky et al. (2012)	Vissapragada et al. (2021)
Kepler-29	2086435189017387264	Kepler-29 c	13.28613	4.5 $^{+1.1}_{-1.1}$	2.34 $^{+0.12}_{-0.11}$	0.032	TTV	Fabrycky et al. (2012)	Vissapragada et al. (2021)
Kepler-450	2135590578620605568	Kepler-450 c	15.4131395	12.5 $^{+3.2}_{-2.6}$	2.60 $^{+0.00}_{-0.00}$	0.032	TTV	Van Eylen & Albrecht (2015)	Yoffe et al. (2021)
Kepler-96	2073731161099713408	Kepler-96 b	16.2385	8.5 $^{+3.4}_{-3.4}$	2.67 $^{+0.22}_{-0.22}$	0.032	Doppler	Marcy et al. (2014)	Marcy et al. (2014)
K2-106	2582617711154563968	EPIC 220674823 b	0.571	7.7 $^{+0.8}_{-0.8}$	1.71 $^{+0.07}_{-0.07}$	0.00064	Doppler	Adams et al. (2017)	Dai et al. (2019)
K2-106	2582617711154563968	EPIC 220674823 c	13.3397	5.8 $^{+3.3}_{-3.3}$	2.50 $^{+0.27}_{-0.26}$	0.031	Doppler	Adams et al. (2017)	Guenther et al. (2017)
K2-110	3613175223837135616	K2-110 b	13.86375	16.7 $^{+3.2}_{-3.2}$	2.59 $^{+0.10}_{-0.10}$	0.03	Doppler	Osborn et al. (2017)	Osborn et al. (2017)
TOI-125	4698692744355471616	TOI-125 b	4.65382	9.5 $^{+0.9}_{-0.9}$	2.73 $^{+0.08}_{-0.08}$	0.0064	Doppler	Quinn et al. (2019)	Nielsen et al. (2020)
TOI-125	4698692744355471616	TOI-125 c	9.15059	6.6 $^{+1.0}_{-1.0}$	2.76 $^{+0.10}_{-0.10}$	0.019	Doppler	Quinn et al. (2019)	Nielsen et al. (2020)
TOI-125	4698692744355471616	TOI-125 d	19.98	13.6 $^{+1.2}_{-1.2}$	2.93 $^{+0.17}_{-0.17}$	0.013	Doppler	Nielsen et al. (2020)	Nielsen et al. (2020)
Kepler-305	2073547954981763328	Kepler-305 d	16.739	9.1 $^{+3.8}_{-3.8}$	2.80 $^{+0.09}_{-0.09}$	0.03	TTV	Rowe et al. (2014)	Hadden & Lithwick (2015)
Kepler-1655	2100392428275714688	Kepler-1655 b	11.8728787	5.0 $^{+3.1}_{-2.8}$	2.21 $^{+0.08}_{-0.08}$	0.029	Doppler	Haywood et al. (2018)	Haywood et al. (2018)
Kepler-85	2127398083121764736	Kepler-85 e	25.215	0.6 $^{+0.5}_{-0.4}$	1.28 $^{+0.09}_{-0.09}$	0.028	TTV	Rowe et al. (2014)	Hadden & Lithwick (2017)
CD-39 7945	6140553127216043648	TOI-763 b	5.6057	9.8 $^{+0.8}_{-0.8}$	2.28 $^{+0.11}_{-0.11}$	0.0093	Doppler	Fridlund et al. (2020)	Fridlund et al. (2020)
CD-39 7945	6140553127216043648	TOI-763 c	12.2737	9.3 $^{+1.0}_{-1.0}$	2.63 $^{+0.12}_{-0.12}$	0.028	Doppler	Fridlund et al. (2020)	Fridlund et al. (2020)
Kepler-307	2073691303802278784	Kepler-307 b	10.416	8.8 $^{+0.9}_{-0.9}$	3.04 $^{+0.07}_{-0.06}$	0.016	TTV	Xie (2014)	Hadden & Lithwick (2017)

Table 1 continued

Table 1 (continued)

Host Star	Gaia DR2	Exoplanet	Period	Mass	Radius	Occurrence	Mass	Discovery	Parameter
Simbad Name	Source ID	Name	(days)	( $M_{\oplus}$ )	( $R_{\oplus}$ )		Method	Reference	Reference
Kepler-307	2073691303802278784	Kepler-307 c	13.084	3.9 $^{+0.7}_{-0.4}$	2.73 $^{+0.06}_{-0.03}$	0.028	TTV	Xie (2014)	Hadden & Lithwick (2017)
Kepler-406	2126601108991279872	Kepler-406 b	2.42629	6.3 $^{+1.4}_{-1.4}$	1.43 $^{+0.03}_{-0.03}$	0.0059	Doppler	Marcy et al. (2014)	Marcy et al. (2014)
Kepler-406	2126601108991279872	Kepler-406 c	4.62332	2.7 $^{+1.8}_{-1.8}$	0.85 $^{+0.03}_{-0.03}$	0.027	Doppler	Marcy et al. (2014)	Marcy et al. (2014)
Kepler-107	2086625752425381632	Kepler-107 b	3.1800218	3.5 $^{+1.5}_{-1.5}$	1.54 $^{+0.02}_{-0.02}$	0.0074	Doppler	Rowe et al. (2014)	Bonomo et al. (2019)
Kepler-107	2086625752425381632	Kepler-107 c	4.901452	9.4 $^{+1.8}_{-1.8}$	1.60 $^{+0.03}_{-0.03}$	0.011	Doppler	Rowe et al. (2014)	Bonomo et al. (2019)
Kepler-107	2086625752425381632	Kepler-107 e	14.749143	8.6 $^{+3.6}_{-3.6}$	2.90 $^{+0.04}_{-0.04}$	0.025	Doppler	Rowe et al. (2014)	Bonomo et al. (2019)
Kepler-454	2099541715513813504	Kepler-454 b	10.57375339	6.8 $^{+1.4}_{-1.4}$	2.37 $^{+0.13}_{-0.13}$	0.025	Doppler	Gottel et al. (2016)	Gottel et al. (2016)
K2-38	6237129658760381056	K2-38 b	4.01593	12.0 $^{+2.9}_{-2.9}$	1.55 $^{+0.16}_{-0.16}$	0.0097	Doppler	Sinkoff et al. (2016)	Sinkoff et al. (2016)
K2-38	6237129658760381056	K2-38 c	10.56103	9.9 $^{+4.6}_{-4.6}$	2.42 $^{+0.29}_{-0.29}$	0.025	Doppler	Sinkoff et al. (2016)	Sinkoff et al. (2016)
Kepler-51	2135275362382289280	Kepler-51 b	45.155	2.3 $^{+1.7}_{-1.6}$	7.47 $^{+0.09}_{-0.16}$	0.0044	TTV	Steffen et al. (2013)	Hadden & Lithwick (2017)
Kepler-51	2135275362382289280	Kepler-51 c	85.316	3.9 $^{+0.8}_{-0.8}$	4.13 $^{+0.10}_{-0.10}$	0.024	TTV	Steffen et al. (2013)	Hadden & Lithwick (2017)
Kepler-51	2135275362382289280	Kepler-51 d	130.18	6.2 $^{+1.6}_{-1.5}$	10.21 $^{+0.12}_{-0.23}$	0.013	TTV	Masuda (2014)	Hadden & Lithwick (2017)
K2-32	4130539180358512768	K2-32 b	8.99213	16.5 $^{+2.7}_{-2.7}$	5.13 $^{+0.28}_{-0.28}$	0.024	Doppler	Dai et al. (2016)	Petigura et al. (2017)
K2-32	4130539180358512768	K2-32 d	31.7154	10.3 $^{+4.7}_{-4.7}$	3.43 $^{+0.35}_{-0.35}$	0.023	Doppler	Dai et al. (2016)	Petigura et al. (2017)
Kepler-100	2101733244046205668	Kepler-100 b	6.88705	7.3 $^{+3.2}_{-3.2}$	1.32 $^{+0.04}_{-0.04}$	0.022	Doppler	Marcy et al. (2014)	Marcy et al. (2014)
HD 97658	399707520623285888	HD 97658 b	9.4903	7.5 $^{+0.8}_{-0.8}$	2.25 $^{+0.10}_{-0.10}$	0.022	Doppler	Howard et al. (2011)	Van Grootel et al. (2016)
HD 106315	3698307419878650240	HD 106315 b	9.55237	12.6 $^{+3.2}_{-3.2}$	2.44 $^{+0.17}_{-0.17}$	0.022	Doppler	Crossfield et al. (2017)	Barros et al. (2017)
HD 106315	3698307419878650240	HD 106315 c	21.05704	15.2 $^{+3.7}_{-3.7}$	4.35 $^{+0.23}_{-0.23}$	0.01	Doppler	Crossfield et al. (2017)	Barros et al. (2017)
Kepler-279	2102456726998624640	Kepler-279 c	35.735	7.4 $^{+2.2}_{-2.2}$	4.25 $^{+0.13}_{-0.13}$	0.013	TTV	Xie (2014)	Hadden & Lithwick (2017)
Kepler-279	2102456726998624640	Kepler-279 d	54.414	4.5 $^{+1.9}_{-1.9}$	3.71 $^{+0.12}_{-0.11}$	0.02	TTV	Xie (2014)	Hadden & Lithwick (2017)
Kepler-19	2051106987063242880	Kepler-19 b	9.28716	8.4 $^{+1.6}_{-1.6}$	2.21 $^{+0.05}_{-0.05}$	0.02	joint	Ballard et al. (2011)	Malavolta et al. (2017)
Kepler-1662	2127790368255394048	KOI-1783.02	284.215	15.0 $^{+4.3}_{-4.3}$	5.44 $^{+0.52}_{-0.52}$	0.02	TTV	Vissapragada et al. (2020)	Vissapragada et al. (2020)
BD-00 4534	2645940376800212096	HIP 116454 b	9.1205	11.8 $^{+1.3}_{-1.3}$	2.53 $^{+0.18}_{-0.18}$	0.02	Doppler	Vanderburg et al. (2015)	Vanderburg et al. (2015)
Kepler-60	2102316985943863424	Kepler-60 b	7.133	3.7 $^{+0.6}_{-0.6}$	1.98 $^{+0.06}_{-0.06}$	0.0098	TTV	Steffen et al. (2013)	Hadden & Lithwick (2017)
Kepler-60	2102316985943863424	Kepler-60 c	8.919	2.0 $^{+0.5}_{-0.5}$	2.21 $^{+0.06}_{-0.06}$	0.019	TTV	Steffen et al. (2013)	Hadden & Lithwick (2017)
Kepler-60	2102316985943863424	Kepler-60 d	11.899	3.9 $^{+0.7}_{-0.6}$	1.89 $^{+0.09}_{-0.10}$	0.013	TTV	Steffen et al. (2013)	Hadden & Lithwick (2017)
HD 219134	2009481748875806976	HD 219134 b	3.092926	4.7 $^{+0.2}_{-0.2}$	1.60 $^{+0.06}_{-0.06}$	0.0062	Doppler	Motalebi et al. (2015)	Hadden & Lithwick (2017)
HD 219134	2009481748875806976	HD 219134 c	6.76458	4.4 $^{+0.2}_{-0.2}$	1.51 $^{+0.05}_{-0.05}$	0.017	Doppler	Motalebi et al. (2015)	Gillon et al. (2017)
CD-61 1276	5481210874877547904	TOI-220 b	10.695264	13.8 $^{+1.0}_{-1.0}$	3.03 $^{+0.15}_{-0.15}$	0.017	Doppler	Hoyer et al. (2021)	Hoyer et al. (2021)
BD+40 3638	2102119176929154304	Kepler-65 b	2.1549209	2.4 $^{+2.4}_{-1.6}$	1.44 $^{+0.04}_{-0.03}$	0.0046	joint	Chaplin et al. (2013)	Mills et al. (2019)
BD+40 3638	2102119176929154304	Kepler-65 c	5.859697	5.4 $^{+1.7}_{-1.7}$	2.62 $^{+0.07}_{-0.07}$	0.01	joint	Chaplin et al. (2013)	Mills et al. (2019)
BD+40 3638	2102119176929154304	Kepler-65 d	8.13167	4.1 $^{+0.8}_{-0.8}$	1.59 $^{+0.04}_{-0.04}$	0.017	joint	Chaplin et al. (2013)	Mills et al. (2019)
Kepler-177	2106339927188171776	Kepler-177 b	36.855	5.4 $^{+1.0}_{-0.9}$	3.92 $^{+0.72}_{-0.61}$	0.016	TTV	Xie (2014)	Hadden & Lithwick (2017)
Kepler-177	2106339927188171776	Kepler-177 c	49.412	13.5 $^{+2.6}_{-2.6}$	8.36 $^{+1.37}_{-1.37}$	0.0041	TTV	Xie (2014)	Hadden & Lithwick (2017)
Kepler-36	2129931456691176576	Kepler-36 b	13.848	3.9 $^{+0.2}_{-0.2}$	1.71 $^{+0.04}_{-0.04}$	0.016	TTV	Carter et al. (2012)	Hadden & Lithwick (2017)
Kepler-36	2129931456691176576	Kepler-36 c	16.233	7.5 $^{+0.3}_{-0.3}$	4.15 $^{+0.07}_{-0.07}$	0.0084	TTV	Carter et al. (2012)	Hadden & Lithwick (2017)
K2-314	6259263137059042048	EPIC 249893012 b	3.5951	8.8 $^{+1.1}_{-1.1}$	1.95 $^{+0.09}_{-0.09}$	0.0038	Doppler	Hidalgo et al. (2020)	Hidalgo et al. (2020)
K2-314	6259263137059042048	EPIC 249893012 c	15.624	14.7 $^{+1.9}_{-1.9}$	3.67 $^{+0.14}_{-0.14}$	0.01	Doppler	Hidalgo et al. (2020)	Hidalgo et al. (2020)
K2-314	6259263137059042048	EPIC 249893012 d	35.747	10.2 $^{+2.4}_{-2.4}$	3.94 $^{+0.13}_{-0.12}$	0.016	Doppler	Hidalgo et al. (2020)	Hidalgo et al. (2020)
Kepler-33	2127355923723254272	Kepler-33 d	21.776	4.1 $^{+1.7}_{-2.0}$	5.37 $^{+0.12}_{-0.13}$	0.004	TTV	Lissauer et al. (2012)	Hadden & Lithwick (2017)

Table 1 continued

Table 1 (continued)

Host Star	Gaia DR2	Exoplanet	Period	Mass	Radius	Occurrence	Mass	Discovery	Parameter
Simbad Name	Source ID	Name	(days)	( $M_{\oplus}$ )	( $R_{\oplus}$ )		( $R_{\oplus}$ )	Reference	Reference
Kepler-33	2127355923723254272	Kepler-33 e	31.784	$5.5^{+1.2}_{-1.1}$	$4.00^{+0.11}_{-0.11}$	0.015		Lissauer et al. (2012)	Hadden & Lithwick (2015)
Kepler-33	2127355923723254272	Kepler-33 f	41.028	$9.6^{+1.7}_{-1.7}$	$4.43^{+0.11}_{-0.11}$	0.011		Lissauer et al. (2012)	Hadden & Lithwick (2015)
Kepler-105	2130368310704421120	Kepler-105 c	7.126	$3.6^{+1.3}_{-1.3}$	$1.60^{+0.04}_{-0.04}$	0.015		Rowe et al. (2014)	Hadden & Lithwick (2015)
Kepler-103	2101243789577188756	Kepler-103 b	15.9654	$9.7^{+8.6}_{-8.6}$	$3.37^{+0.09}_{-0.09}$	0.015		Marcy et al. (2014)	Marcy et al. (2014)
Kepler-103	2101243789577188756	Kepler-103 c	179.612	$36.1^{+25.2}_{-25.2}$	$5.14^{+0.14}_{-0.14}$	0.011		Marcy et al. (2014)	Marcy et al. (2014)
Kepler-82	2125850623586710400	Kepler-82 b	26.44	$12.2^{+1.0}_{-1.0}$	$4.07^{+0.24}_{-0.24}$	0.015		Xie (2013)	Freudenthal et al. (2019)
Kepler-82	2125850623586710400	Kepler-82 c	51.54	$13.9^{+1.3}_{-1.2}$	$5.34^{+0.32}_{-0.13}$	0.0053		Xie (2013)	Freudenthal et al. (2019)
Kepler-1659	2073779161653824640	KOI-1599.01	20.4415	$4.6^{+0.3}_{-0.3}$	$1.90^{+0.30}_{-0.30}$	0.01		Panichi et al. (2019)	Panichi et al. (2019)
Kepler-1659	2073779161653824640	KOI-1599.02	13.6088	$9.0^{+0.3}_{-0.3}$	$1.90^{+0.20}_{-0.20}$	0.013		Panichi et al. (2019)	Panichi et al. (2019)
BD+38 3583	2052747119115620352	Kepler-93 b	4.72673978	$4.0^{+0.7}_{-0.7}$	$1.48^{+0.02}_{-0.02}$	0.013		Marcy et al. (2014)	Dressing & Charbonneau (2015)
HD 183579	6641996571978861440	HD 183579 b	17.471278	$19.7^{+3.0}_{-3.0}$	$3.55^{+0.15}_{-0.15}$	0.013		Palatnick et al. (2021)	Palatnick et al. (2021)
K2-10	3798690151434945280	K2-10 b	19.3044	$27.0^{+17.0}_{-16.0}$	$3.84^{+0.35}_{-0.34}$	0.013		Montet et al. (2015)	Van Eylen et al. (2016)
Kepler-99	2076871091425583232	Kepler-99 b	4.60358	$6.2^{+1.3}_{-1.3}$	$1.48^{+0.08}_{-0.08}$	0.013		Marcy et al. (2014)	Marcy et al. (2014)
Kepler-25	2100451630105041152	Kepler-25 b	6.238297	$8.7^{+2.5}_{-2.3}$	$2.75^{+0.04}_{-0.04}$	0.012		Steffen et al. (2012)	Mills et al. (2019)
Kepler-25	2100451630105041152	Kepler-25 c	12.7207	$15.2^{+1.6}_{-1.6}$	$5.22^{+0.06}_{-0.07}$	0.0033		Steffen et al. (2012)	Mills et al. (2019)
Kepler-87	2086306584816171392	Kepler-87 c	191.2318	$6.4^{+0.8}_{-0.8}$	$6.14^{+0.29}_{-0.29}$	0.01		Ofir et al. (2014)	Ofir et al. (2014)
* pi. Men	462303686537393408	pi Men c	6.2679	$4.8^{+0.8}_{-0.9}$	$2.04^{+0.05}_{-0.05}$	0.009		Gandolfi et al. (2018)	Huang et al. (2018)
Kepler-95	210670526998803072	Kepler-95 b	11.5231	$13.0^{+2.9}_{-2.9}$	$3.42^{+0.09}_{-0.09}$	0.0087		Marcy et al. (2014)	Marcy et al. (2014)
BD-14 1137	2984582227215748864	TOI-421 b	5.19672	$7.2^{+0.7}_{-0.7}$	$2.68^{+0.19}_{-0.19}$	0.0082		Carleo et al. (2020)	Carleo et al. (2020)
BD-14 1137	2984582227215748864	TOI-421 c	16.06819	$16.4^{+1.1}_{-1.0}$	$5.09^{+0.16}_{-0.15}$	0.0038		Carleo et al. (2020)	Carleo et al. (2020)
K2-66	2614121364991061888	K2-66 b	5.06963	$21.3^{+3.6}_{-3.6}$	$2.49^{+0.24}_{-0.24}$	0.0078		Crossfield et al. (2016)	Sinukoff et al. (2017)
Kepler-88	2101507367429089664	KOI-142 b	10.91647	$9.5^{+1.1}_{-1.1}$	$3.44^{+0.08}_{-0.08}$	0.0078		Weiss et al. (2021)	Weiss et al. (2021)
K2-111	5300669599267328	K2-111 b	5.3518	$5.3^{+0.8}_{-0.8}$	$1.82^{+0.11}_{-0.09}$	0.0074		Fridlund et al. (2017)	Mortier et al. (2020)
Kepler-113	2133369840008452224	Kepler-113 b	4.754	$11.7^{+4.2}_{-4.2}$	$1.82^{+0.05}_{-0.06}$	0.0064		Marcy et al. (2014)	Marcy et al. (2014)
Kepler-89	2076970047474270208	KOI-94 b	3.743208	$10.5^{+4.6}_{-4.6}$	$1.71^{+0.16}_{-0.16}$	0.0064		Weiss et al. (2013)	Weiss et al. (2013)
Kepler-89	2076970047474270208	KOI-94 c	10.424	$7.8^{+2.4}_{-2.4}$	$4.32^{+0.10}_{-0.09}$	0.0044		Weiss et al. (2013)	Hadden & Lithwick (2017)
Kepler-89	2076970047474270208	KOI-94 e	54.32031	$35.0^{+18.0}_{-18.0}$	$6.56^{+0.62}_{-0.62}$	0.0052		Weiss et al. (2013)	Weiss et al. (2013)
Kepler-97	2131216137248338304	Kepler-97 b	2.58664	$3.5^{+1.9}_{-1.9}$	$1.48^{+0.13}_{-0.13}$	0.006		Marcy et al. (2014)	Marcy et al. (2014)
K2-36	3811989156889528320	K2-36 b	1.422614	$3.9^{+1.1}_{-1.1}$	$1.43^{+0.08}_{-0.08}$	0.0019		Sinukoff et al. (2016)	Damasso et al. (2019)
K2-36	3811989156889528320	K2-36 c	5.340888	$7.8^{+2.3}_{-2.3}$	$3.20^{+0.30}_{-0.30}$	0.0052		Sinukoff et al. (2016)	Damasso et al. (2019)
WASP-47	2613413008919918976	WASP-47 d	9.03077	$13.1^{+1.5}_{-1.5}$	$3.58^{+0.05}_{-0.05}$	0.005		Becker et al. (2015)	Vanderburg et al. (2017)
WASP-47	2613413008919918976	WASP-47 e	0.789592	$6.8^{+0.7}_{-0.7}$	$1.81^{+0.03}_{-0.03}$	0.00043		Becker et al. (2015)	Vanderburg et al. (2017)
HD 86226	5660492297395345408	HD 86226 c	3.98442	$7.2^{+1.2}_{-1.1}$	$2.16^{+0.08}_{-0.08}$	0.0048		Teske et al. (2020b)	Teske et al. (2020b)
HD 179070	2099606483621385216	Kepler-21 b	2.78578	$5.1^{+1.7}_{-1.7}$	$1.64^{+0.02}_{-0.02}$	0.0048		Howell et al. (2012)	López-Morales et al. (2015)
K2-105	651907079835937280	K2-105 b	8.266902	$30.0^{+19.0}_{-19.0}$	$3.59^{+0.42}_{-0.42}$	0.0045		Narita et al. (2017)	Narita et al. (2017)
K2-98	601199802584914816	K2-98 b	10.13675	$32.2^{+8.1}_{-8.1}$	$4.30^{+0.30}_{-0.20}$	0.0043		Barragán et al. (2016)	Barragán et al. (2016)
CD-24 12681	6049750234317822208	K2-24 b	20.88977	$19.0^{+2.2}_{-2.1}$	$5.40^{+0.20}_{-0.20}$	0.0039		Petigura et al. (2016)	Petigura et al. (2018)
CD-24 12681	6049750234317822208	K2-24 c	42.3391	$15.4^{+1.8}_{-1.8}$	$7.50^{+0.30}_{-0.30}$	0.0042		Petigura et al. (2016)	Petigura et al. (2018)
Kepler-223	2086337508581280256	Kepler-223 b	7.385	$4.0^{+2.1}_{-2.1}$	$3.94^{+0.43}_{-0.43}$	0.0035		Rowe et al. (2014)	Hadden & Lithwick (2017)
Kepler-223	2086337508581280256	Kepler-223 c	9.848	$12.4^{+2.8}_{-2.9}$	$4.34^{+0.50}_{-0.48}$	0.004		Rowe et al. (2014)	Hadden & Lithwick (2017)

Table 1 continued

Table 1 (continued)

Host Star	Gaia DR2	Exoplanet	Period	Mass	Radius	Occurrence	Mass	Discovery	Parameter
Simbad Name	Source ID	Name	(days)	( $M_{\oplus}$ )	( $R_{\oplus}$ )			Reference	Reference
Kepler-223	2086337508581280256	Kepler-223 d	14.787	$5.9^{+1.9}_{-1.2}$	$5.87^{+0.61}_{-0.06}$	0.0028	TTV	Rowe et al. (2014)	Hadden & Lithwick (2017)
K2-285	2657374606238804992	K2-285 b	3.471745	$9.7^{+1.2}_{-1.4}$	$2.59^{+0.06}_{-0.06}$	0.0028	Doppler	Palle et al. (2019)	Palle et al. (2019)
K2-285	2657374606238804992	K2-285 c	7.138048	$15.7^{+2.3}_{-2.1}$	$3.53^{+0.08}_{-0.08}$	0.0039	Doppler	Palle et al. (2019)	Palle et al. (2019)
K2-19	3798833775141351552	K2-19 b	7.9194	$28.5^{+5.4}_{-5.0}$	$7.74^{+0.39}_{-0.39}$	0.00089	Doppler	Dai et al. (2016)	Dai et al. (2016)
K2-19	3798833775141351552	K2-19 c	11.90715	$25.6^{+7.1}_{-6.9}$	$4.86^{+0.61}_{-0.44}$	0.0038	Doppler	Dai et al. (2016)	Dai et al. (2016)
HD 285181	3409148746676599168	K2-291 b	2.225177	$6.5^{+1.2}_{-1.2}$	$1.59^{+0.10}_{-0.07}$	0.0036	Doppler	Kosiarek et al. (2019)	Kosiarek et al. (2019)
CoRoT-24	3105404467618982272	CoRoT-24 c	11.759	$28.0^{+11.0}_{-11.0}$	$5.00^{+0.50}_{-0.50}$	0.0034	Doppler	Alonso et al. (2014)	Alonso et al. (2014)
Kepler-46	2102700131386216576	Kepler-46 b	33.648	$28.1^{+106.0}_{-106.0}$	$7.99^{+0.19}_{-0.19}$	0.0033	TTV	Nesvorný et al. (2012)	Saad-Oliveira et al. (2017)
BD-15 6276	2597119620985658496	K2-265 b	2.369172	$6.5^{+0.8}_{-0.8}$	$1.77^{+0.11}_{-0.11}$	0.0031	Doppler	Lam et al. (2018)	Lam et al. (2018)
BD+19 2158	636363799347569408	EPIC 211945201 b	19.49213	$27.0^{+14.0}_{-12.6}$	$6.12^{+0.10}_{-0.10}$	0.003	Doppler	Chakrabarty et al. (2018)	Chakrabarty et al. (2018)
CoRoT-22	4285572454508522496	CoRoT-22 b	9.75598	$12.2^{+44.0}_{-44.0}$	$4.88^{+0.37}_{-0.37}$	0.003	Doppler	Moutou et al. (2014)	Moutou et al. (2014)
TOI-216	4664811297844004352	TOI-216.01	34.556	$200.0^{+170.0}_{-100.0}$	$11.29^{+0.58}_{-0.58}$	0.0029	TTV	Kipping et al. (2019)	Kipping et al. (2019)
TOI-216	4664811297844004352	TOI-216.02	17.089	$30.0^{+20.0}_{-14.0}$	$7.69^{+1.62}_{-0.83}$	0.0018	TTV	Kipping et al. (2019)	Kipping et al. (2019)
HD 158259	1416050859226670848	HD 158259 b	2.178	$2.2^{+0.4}_{-0.4}$	$1.20^{+1.30}_{-0.13}$	0.0028	Doppler	Hara et al. (2020)	Hara et al. (2020)
Kepler-18	2079295583282164992	Kepler-18 d	14.859	$14.9^{+4.2}_{-4.2}$	$5.93^{+0.06}_{-0.06}$	0.0027	TTV	Cochran et al. (2011)	Hadden & Lithwick (2017)
K2-27	379852815560689792	K2-27 b	6.771315	$30.9^{+4.6}_{-4.6}$	$4.48^{+0.23}_{-0.23}$	0.0024	Doppler	Van Eylen et al. (2016)	Petigura et al. (2017)
K2-216	2556231154370582400	K2-216 b	2.1748	$8.0^{+1.6}_{-1.6}$	$1.75^{+0.17}_{-0.10}$	0.0024	Doppler	Mayo et al. (2018)	Persson et al. (2018)
HD 110113	6133384959942131968	HD 110113 b	2.541	$4.5^{+0.6}_{-0.6}$	$2.05^{+0.12}_{-0.12}$	0.002	Doppler	Osborn et al. (2021)	Osborn et al. (2021)
Kepler-117	2130959744881558272	Kepler-117 b	18.7959228	$29.9^{+10.5}_{-10.5}$	$8.06^{+0.27}_{-0.27}$	0.002	joint	Rowe et al. (2014)	Bruno et al. (2015)
HD 219666	6492940453524576128	HD 219666 b	6.03607	$16.6^{+1.3}_{-1.3}$	$4.71^{+0.17}_{-0.17}$	0.0019	Doppler	Esposito et al. (2019)	Esposito et al. (2019)
BD-05 3504	3583630929786305280	K2-229 b	0.584	$2.5^{+0.4}_{-0.4}$	$1.20^{+0.04}_{-0.04}$	0.0017	Doppler	Mayo et al. (2018)	Dai et al. (2019)
Kepler-78	2078373642776670080	Kepler-78 b	0.355	$1.8^{+0.2}_{-0.2}$	$1.23^{+0.02}_{-0.02}$	0.0016	Doppler	Sanchis-Ojeda et al. (2013)	Dai et al. (2019)
TYC 4450-1307-1	2274696151198328960	TOI-1444 b	0.4702694	$3.9^{+0.7}_{-0.7}$	$1.40^{+0.06}_{-0.06}$	0.0015	Doppler	Dai et al. (2021)	Dai et al. (2021)
SAKM 1-2122	2643952940813536768	K2-141 b	0.2803244	$5.1^{+0.4}_{-0.4}$	$1.51^{+0.05}_{-0.05}$	0.0012	Doppler	Malavolta et al. (2018)	Malavolta et al. (2018)
Kepler-4	2132152916856093952	Kepler-4 b	3.21346	$24.5^{+3.8}_{-3.8}$	$4.00^{+0.21}_{-0.21}$	0.0012	Doppler	Borucki et al. (2010)	Borucki et al. (2010)
HD 89345	3877070590167177344	HD 89345 b	11.8143	$35.0^{+5.4}_{-5.7}$	$7.40^{+0.31}_{-0.34}$	0.0011	Doppler	Van Eylen et al. (2018)	Yu et al. (2018)
HATS-46	4919771654727611008	HATS-46 b	4.7423729	$55.0^{+19.7}_{-19.7}$	$10.12^{+0.65}_{-0.50}$	0.0011	Doppler	Brahm et al. (2018)	Brahm et al. (2018)
CoRoT-32	3326541506073371776	CoRoT-32 b	6.71837	$47.7^{+31.8}_{-31.8}$	$6.39^{+0.56}_{-0.56}$	0.001	Doppler	Bouffeur et al. (2018)	Bouffeur et al. (2018)
Kepler-94	2119602202081351168	Kepler-94 b	2.50806	$10.8^{+1.4}_{-1.4}$	$3.57^{+0.15}_{-0.15}$	0.00099	Doppler	Marcy et al. (2014)	Marcy et al. (2014)
CoRoT-7	310726717757848576	CoRoT-7 b	0.854	$4.6^{+1.1}_{-1.2}$	$1.58^{+0.10}_{-0.10}$	0.00099	Doppler	Léger et al. (2009)	Dai et al. (2019)
BD-09 6003	2609222216055014144	K2-39 b	4.60497	$39.8^{+4.4}_{-4.4}$	$5.71^{+0.63}_{-0.63}$	0.00093	Doppler	Van Eylen et al. (2016)	Petigura et al. (2017)
HD 80653	606477252238780160	HD 80653 b	0.719573	$5.6^{+0.4}_{-0.4}$	$1.67^{+0.07}_{-0.07}$	0.00087	Doppler	Frustagli et al. (2020)	Frustagli et al. (2020)
Gaia DR2 6585082036193768832	6585082036193768832	NGTS-14 A b	3.5357173	$29.2^{+3.8}_{-3.8}$	$4.98^{+0.34}_{-0.34}$	0.00079	Doppler	Smith et al. (2021)	Smith et al. (2021)
K2-131	358092087843798688	K2-131 b	0.369	$6.3^{+1.4}_{-1.4}$	$1.65^{+0.06}_{-0.06}$	0.00077	Doppler	Dai et al. (2017)	Dai et al. (2019)
HAT-P-26	3668036348641580288	HAT-P-26 b	4.234516	$18.8^{+2.2}_{-2.2}$	$6.33^{+0.36}_{-0.36}$	0.00074	Doppler	Hartman et al. (2011)	Hartman et al. (2011)
CD-44 14956	6520880040423258240	TOI-132 b	2.1097019	$22.4^{+1.9}_{-1.9}$	$3.42^{+0.13}_{-0.14}$	0.00074	Doppler	Díaz et al. (2020)	Díaz et al. (2020)
HATS-37	6194574671813047424	HATS-37 A b	4.3315366	$31.5^{+13.3}_{-13.3}$	$6.79^{+0.18}_{-0.18}$	0.00066	Doppler	Jordán et al. (2020)	Jordán et al. (2020)
HD 213885	6407428994690988928	HD 213885 b	1.008035	$8.8^{+0.6}_{-0.6}$	$1.75^{+0.05}_{-0.05}$	0.00065	Doppler	Espinoza et al. (2020)	Espinoza et al. (2020)
TYC 6022-794-1	5472386851683941376	HATS-38 b	4.375021	$23.5^{+3.5}_{-3.5}$	$6.88^{+0.19}_{-0.19}$	0.00064	Doppler	Jordán et al. (2020)	Jordán et al. (2020)
Kepler-98	2099862910348755712	Kepler-98 b	1.54168	$3.5^{+1.6}_{-1.6}$	$1.99^{+0.22}_{-0.22}$	0.00058	Doppler	Marcy et al. (2014)	Marcy et al. (2014)

Table 1 continued

Table 1 (*continued*)

Host Star	Gaia DR2	Exoplanet	Period	Mass	Radius	Occurrence	Mass	Discovery	Parameter
Simbad Name	Source ID	Name	(days)	( $M_{\oplus}$ )	( $R_{\oplus}$ )		Method	Reference	Reference
NGTS-4	2891248292906892032	NGTS-4 b	1.3373508	$20.6^{+3.0}_{-3.0}$	$3.18^{+0.26}_{-0.26}$	0.00041	Doppler	West et al. (2019)	West et al. (2019)
TYC 8688-915-1	5880886001621564928	TOI-824 b	1.392978	$18.5^{+1.8}_{-1.9}$	$2.93^{+0.20}_{-0.19}$	0.00035	Doppler	Burt et al. (2020)	Burt et al. (2020)
* rho01 Cnc	704967037090946688	55 Cnc e	0.7365474	$8.0^{+0.3}_{-0.3}$	$1.88^{+0.03}_{-0.03}$	0.00027	Doppler	McArthur et al. (2004)	Bouffleur et al. (2018)

NOTE—This table is ordered in descending order of the maximum occurrence of individual exoplanets in an exoplanet system. It is available in its entirety in a machine-readable format.